doi.org/10.26434/chemrxiv.12732011.v1

1,2-Dicarbonyl Radicals with Exceptional Physiological and Chemical Stability

Youngsuk Kim, Jung Eun Byeon, Gu Yoon Jeong, Seoung Su Kim, Hayoung Song, Eunsung Lee

Submitted date: 29/07/2020 • Posted date: 29/07/2020

Citation information: Kim, Youngsuk; Byeon, Jung Eun; Jeong, Gu Yoon; Kim, Seoung Su; Song, Hayoung; Lee, Eunsung (2020): 1,2-Dicarbonyl Radicals with Exceptional Physiological and Chemical Stability. ChemRxiv. Preprint. https://doi.org/10.26434/chemrxiv.12732011.v1

The present manuscript describes the design, synthesis, and characterization of the most stable organic radical reported up to date.
Here we report:▪ Synthesis and full characterization including X-ray structure of stable 1,2-dicarbonyl radicals▪ Proposed mechanism for the formation of the presented radicals▪ Redox reactivity of the radicals▪ Stability of the radicals under various organic and inorganic conditions▪ Demonstration of the radicals as potential organic radical contrast agent candidate

1,2-Dicarbonyl Radicals with Exceptional Physiological and Chemical Stability

Youngsuk Kim, Jung Eun Byeon, Gu Yoon Jeong, Seoung Su Kim, Hayoung Song, Eunsung Lee*

Department of Chemistry, Pohang University of Science and Technology (POSTECH), Pohang, 37673, Republic of Korea

Abstract: Organic radicals have been of great academic interest due to their unique reactivity and potential applicability; however, lack of stability and solubility continues to limit their application, especially in physiological conditions. For example, well-known aminoxyl radicals have half-life of a few minutes in physiological conditions due to biological redox active reagents, while shielding using polymeric or supramolecular protecting groups increases their half-life up to several hours. Here we designed and synthesized a new small molecular organic radical based on 1,2-dicarbonyl scaffold with exceptional stability. The presented radicals showed superior stability over present organic radicals towards physiological conditions (half-life of ~3000 hours) and even resistant towards chemically reducing, oxidizing, acidic, basic conditions, and high temperature, without additional protection.

Having an unpaired valence electron, organic radicals are often thermodynamically and kinetically unstable, making their isolation and structural characterization challenging. Since the 'radical' discovery of the triphenylmethyl radical – the first persistent organic radical – by Gomberg in 1900,[1] various strategies to stabilize organic radicals have been developed, leading to the successful discovery of other stable organic radicals (**Figure 1A**).[2] Despite the great potential of air- and water-stable organic radicals as electron transfer reagents, spin labels, or bio-imaging agents, they have limited stability under physiological conditions, which makes a major drawback for bio-application.[3] For example, the most widely studied aminoxyl radicals (also known as nitroxyl radicals) are susceptible to decomposition in the presence of organic or biological reducing agents such as ascorbate, while triarylmethyl radicals readily react with oxidants such as peroxides.[4] Therefore, development of new organic radical platform is desired with high stability towards physiological conditions.

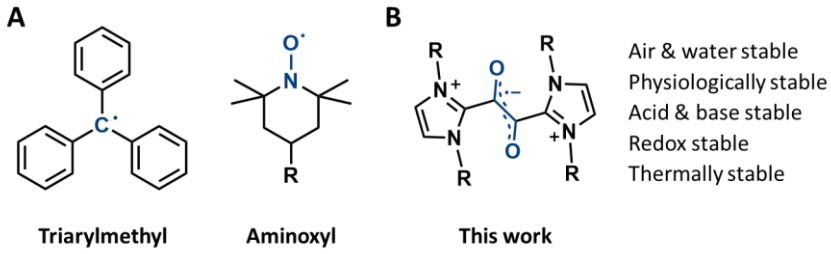

Figure 1. Examples of stable organic radicals.
(A) State of the art examples of most widely used organic radicals.
(B) Stable 1,2-dicarbonyl radicals from this work with the glyoxal radical anion core structure.

π-Conjugation enables the delocalization of spin density and hence increases radical stability.[5] For example, glyoxal derivatives, as one of the simplest π-conjugated molecules, have been reported to generate corresponding 1,2-dicarbonyl radical anions,[6] which are well-known redox active ligands. Several metal complexes containing 1,2-dicarbonyl radical anions have been reported;[7] however, free 1,2-dicarbonyl radical anions are unstable, and have only been studied by spectroscopic and computational methods. For example, one electron reduction of phenylglyoxal derivatives produced the corresponding 1,2-dicarbonyl radical anions which were detected by electron paramagnetic resonance (EPR).[6] Nonetheless, we assumed that, with appropriate steric and electronic stabilization, 1,2-dicarbonyl can be a versatile organic radical fragment.

N-heterocyclic carbenes (NHCs)[8] are well known to facilitate the generation and utilization of unstable species,[9] including main group[10] and organic radicals, including carbonyl,[11] propargyl,[12] and aminyl[13] derivatives, for example. in this context, we designed 1,2-dicarbonyl radical supported by two NHCs which may provide steric protection and delocalization of the spin density (**Figure 1B**).

Herein we report the synthesis and characterization of highly stable 1,2-dicarbonyl radicals with two imidazolium substituents. The presented radical has two major advantages over the widely used nitroxyl radicals: (i) it survives in the physiological reducing conditions while nitroxyl radicals rapidly decomposed to hydroxylamines, (ii) it has negligible spin density on the nitrogen and hydrogen atoms which results in a narrower EPR signal – and enables higher signal to noise ratio – compared to nitroxyl radicals. High stability and water solubility enabled the demonstration of those radicals as potential organic radical contrast agent candidates for magnetic resonance imaging.

Results and discussion

The 1,2-dicarbonyl radicals **2a**$^{\bullet+}$ and **2b**$^{\bullet+}$ can be easily synthesized from oxalyl chloride and the corresponding N-heterocyclic carbenes (NHCs) (**Figure 2A**). Under a N_2 atmosphere, the reaction of NHC **1a** (IMes; 1,3-dimesitylimidazol-2-ylidene) or **1b** (IDipp; 1,3-bis-(2,6-diisopropylphenyl)imidazol-2-ylidene) with substoichiometric amount of oxalyl chloride in THF produced [**2a**$^{\bullet+}$][Cl^-] or [**2b**$^{\bullet+}$][Cl^-], and subsequent anion exchange afforded [**2a**$^{\bullet+}$][BF_4^-] or [**2b**$^{\bullet+}$][BF_4^-], respectively, as deep purple solids. The reaction involves the formation of the dication intermediate [**2a**$^{2+}$][Cl^-]$_2$, followed by a spontaneous one electron reduction (See Supplementary Materials for detail).

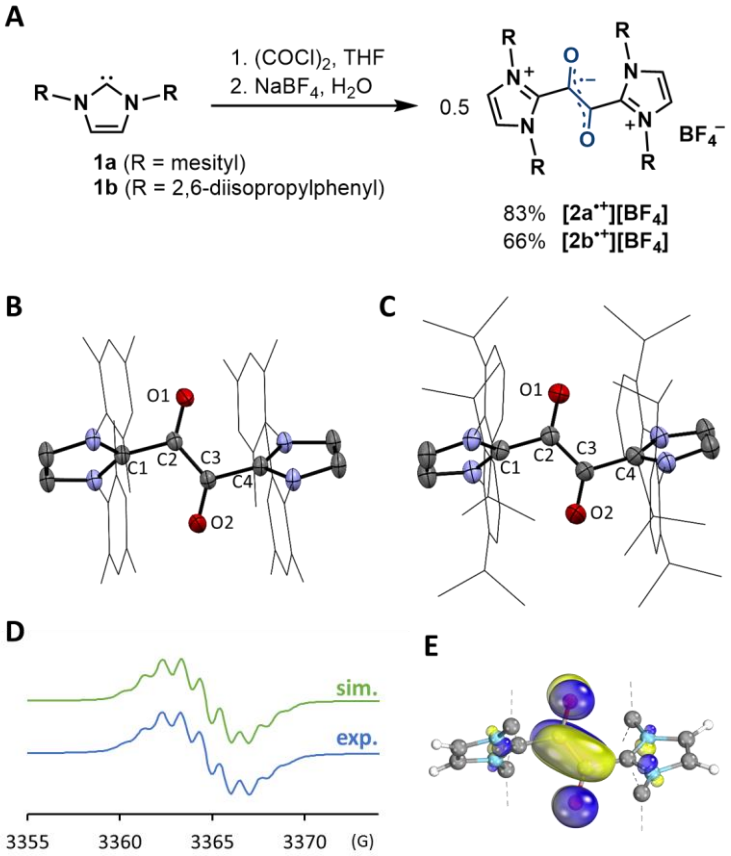

Figure 2. Synthesis and characterization of 1,2-dicarbonyl radicals.
(A) Synthesis of [**2a**$^{\bullet+}$][BF_4^-] and [**2b**$^{\bullet+}$][BF_4^-] from NHCs and oxalyl chloride.
(B and C) Solid-state structure of (B) [**2a**$^{\bullet+}$][BF_4^-] and (C) [**2b**$^{\bullet+}$][BF_4^-] from single crystal X-ray crystallography. The thermal ellipsoids are shown at the 30% probability level. Anions, hydrogen atoms, solvent molecules and disorders were omitted for clarity.
(D) Experimental (bottom) and simulated (top) EPR spectra of [**2a**$^{\bullet+}$][BF_4^-] (g = 2.0060; hyperfine coupling constants: $a(^{14}N)$ = 3.0, 3.0, 2.6, 2.6 MHz).
(E) DFT calculated SOMO(α) of **2a**$^{\bullet+}$ (M06/Def2-SV(P); mesityl substituents were omitted for clarity.

Single crystals suitable for X-ray crystallography were grown by slowly evaporating the mixed water/acetone solutions, enabling the determination of molecular structures of [**2a**$^{\bullet+}$][BF_4^-] and [**2b**$^{\bullet+}$][BF_4^-] (**Figure 2B, 2C** and **Table S1**). The structural parameters for [**2a**$^{\bullet+}$][BF_4^-] and [**2b**$^{\bullet+}$][BF_4^-] are almost identical and well reproduced with DFT calculation on M06/Def2-SV(P)

level of theory (**Table S2**). The bond lengths of the central C_2O_2 unit indicate a bond order of 1.5 (O1–C2 1.245(2) Å; C2–C3 1.411(4) Å; C3–O2 1.245(2) Å for [**2a**$^{\bullet+}$][BF_4^-]). The planar structure of the central C_2O_2 unit also suggests π-delocalization of the radical (torsion angle for O1–C2–C3–O2: 172.8(3)° for [**2a**$^{\bullet+}$][BF_4^-]). The Wiberg bond orders were calculated, which were consistent with the single crystal X-ray structures (O1–C2 1.89; C2–C3 1.22; C3–O2 1.89 for [**2a**$^{\bullet+}$][BF_4^-], **Figure S3**).

Typically, NHC derived radicals[14] have delocalized spin density due to strong π accepting ability of NHCs.[15] In contrast, DFT calculations suggest that **2a**$^{\bullet+}$ and **2b**$^{\bullet+}$ are very rare examples of NHC-derived radicals with minimal delocalization of spin density over the NHC fragments. Very interestingly, 98% of spin density of **2a**$^{\bullet+}$ is localized on the central C_2O_2 unit (O1 32%; C2 17%; C3 17%; O2 32%), with ca. ~1% of spin density for the NHC nitrogen atoms. Experimental EPR spectra of [**2a**$^{\bullet+}$][BF_4^-] and [**2b**$^{\bullet+}$][BF_4^-] were nearly identical, and successfully simulated with hyperfine coupling from four nitrogen atoms with small coupling constants ($a(^{14}N)$ = 3.0, 3.0, 2.6, 2.6 MHz for [**2a**$^{\bullet+}$][BF_4^-]), in agreement with the small spin density on the nitrogen atoms (**Figure 2D**). DFT calculated singly occupied molecular orbital (SOMO) of **2a**$^{\bullet+}$ (**Figure 2E**) well reproduced the typical Ψ_3 orbital of a conjugated system with four *p* orbitals (e.g. 1,3-butadiene). The UV-vis absorption spectrum of [**2a**$^{\bullet+}$][Cl^-] in distilled water at room temperature showed a peak at λ_{max} = 472 nm which was well approximated by time-dependent DFT calculation at M06/Def2-SV(P) level of theory (calculated λ_{max} = 461 nm corresponding to SOMO(α) to LUMO(α) transition, **Figure S10**). Interestingly, [**2a**$^{\bullet+}$][Cl^-] shows weak solvatochromism as its absorption was red-shifted in organic solvents (λ_{max} = 510 nm in acetonitrile; λ_{max} = 521 nm in dichloromethane, **Figure S11**).

The cyclic voltammograms of [**2a**$^{\bullet+}$][BF_4^-] and [**2b**$^{\bullet+}$][BF_4^-] were measured in acetonitrile, which showed reversible redox peaks at $E_{1/2}$ = 0.516 and 0.490 V, respectively (vs. saturated Ag/AgCl electrode, **Figure 3B** and **Figure S6**). Chemical oxidation of [**2a**$^{\bullet+}$][BF_4^-] was performed using $AgBF_4$ as an oxidant, which produced the dication [**2a**$^{2+}$][BF_4^-]$_2$ (**Figure 3A**). Single crystal X-ray structure of [**2a**$^{2+}$][BF_4^-]$_2$ (**Figure 3C**) showed shortened O1–C2 (1.191(2) Å) and C3–O2 (1.201(2) Å), and elongated C2–C3 (1.536(5) Å) bonds, compared to [**2a**$^{\bullet+}$][BF_4^-]. This can be rationalized by considering the removal of the unpaired electron from the Ψ_3 shape SOMO that enhances the bonding O1–C2, C3–O2 and antibonding C2–C3 interactions. In addition, torsion angle for O1–C2–C3–O2 was significantly reduced to 156.9(4)° (compared to 172.8(3)° for [**2a**$^{\bullet+}$][BF_4^-]), which also indicates the decrease of C2–C3 *π* bonding interaction. Calculated Wiberg bond indices of **2a**$^{2+}$ also showed increased bond order for O1–C2 (2.27), C3–O2 (2.29), and decreased bond order for C2–C3 (0.97) compared to **2a**$^{\bullet+}$ (**Figure S3**). On the other hand, electrochemical or chemical reduction of **2a**$^{\bullet+}$ and **2b**$^{\bullet+}$ to the corresponding neutral compounds was not successful.

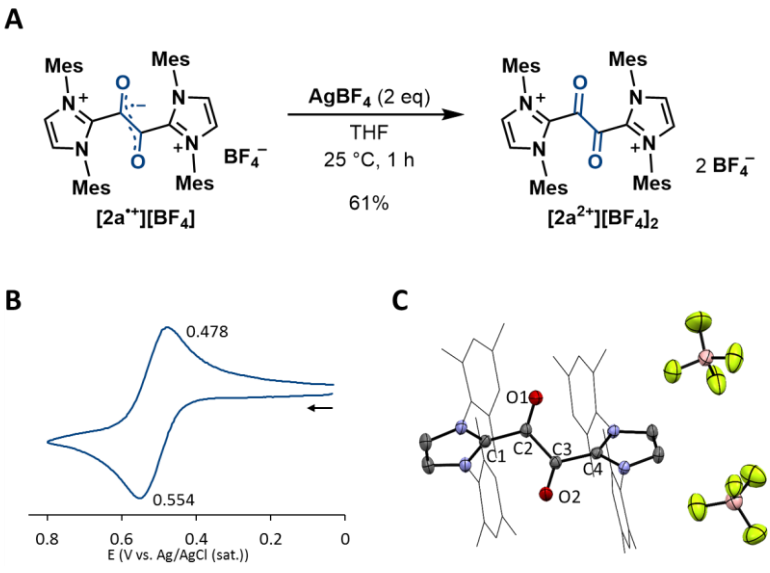

Figure 3. Redox behavior of the 1,2-dicarbonyl radical.

(A) One electron oxidation of [**2a**$^{\bullet+}$][BF_4^-] using silver tetrafluoroborate to produce [**2a**$^{2+}$][BF_4^-]$_2$.

(B) Cyclic voltammogram of [**2a**$^{\bullet+}$][BF_4^-] in acetonitrile with Bu_4NPF_6 (0.1 M) as the supporting electrolyte (scan rate = 0.1 V/s).

(C) Solid-state structure of [**2a**$^{2+}$][BF_4^-]$_2$ from single crystal X-ray crystallography. The thermal ellipsoids are shown at the 30% probability level. Hydrogen atoms, solvent molecules and disorders were omitted for clarity.

To test the stability of 1,2-dicarbonyl radicals under physiological conditions, UV-vis spectrum of [**2a**$^{\bullet+}$][Cl$^-$] solution in potassium phosphate buffer (0.1 M, pH 7.4) was monitored, which showed a peak at λ_{max} = 472 nm. Surprisingly, [**2a**$^{\bullet+}$][Cl$^-$] showed high stability as less than 3% of the radical was decomposed over 7 days which corresponds to the half-life of ~4000 hours (**Figure 4A** and **Figure S12A**). In addition, even in the presence of excess sodium ascorbate in the buffer solution, [**2a**$^{\bullet+}$][Cl$^-$] showed high stability showing the half-life of ~3000 hours (**Figure S12B**). Furthermore, [**2a**$^{\bullet+}$][Cl$^-$] survived in harsher conditions that most other organic radicals cannot (**Figure 4B** and **Figure S13**). For example, solution of [**2a**$^{\bullet+}$][Cl$^-$] in horse blood serum showed ca. 2% decrease of UV-vis absorption over 500 minutes. [**2a**$^{\bullet+}$][Cl$^-$] also showed exceptional stability towards highly basic or oxidizing conditions as in 0.1 M aqueous hydrogen peroxide or 0.1 M aqueous sodium hydroxide, less than 2% of [**2a**$^{\bullet+}$][Cl$^-$] was decomposed over 500 minutes. In the presence of high excess (0.5 M) thiophenol in dichloromethane solution, ~25% decomposition of [**2a**$^{\bullet+}$][Cl$^-$] was observed after 500 minutes, while under 0.1 M aqueous formic acid, ~15% of [**2a**$^{\bullet+}$][Cl$^-$] was decomposed during 500 minutes. while. Notably, [**2a**$^{\bullet+}$][Cl$^-$] showed ~2 hours of half-life even in highly acidic 0.1 M aqueous sulfuric acid solution.

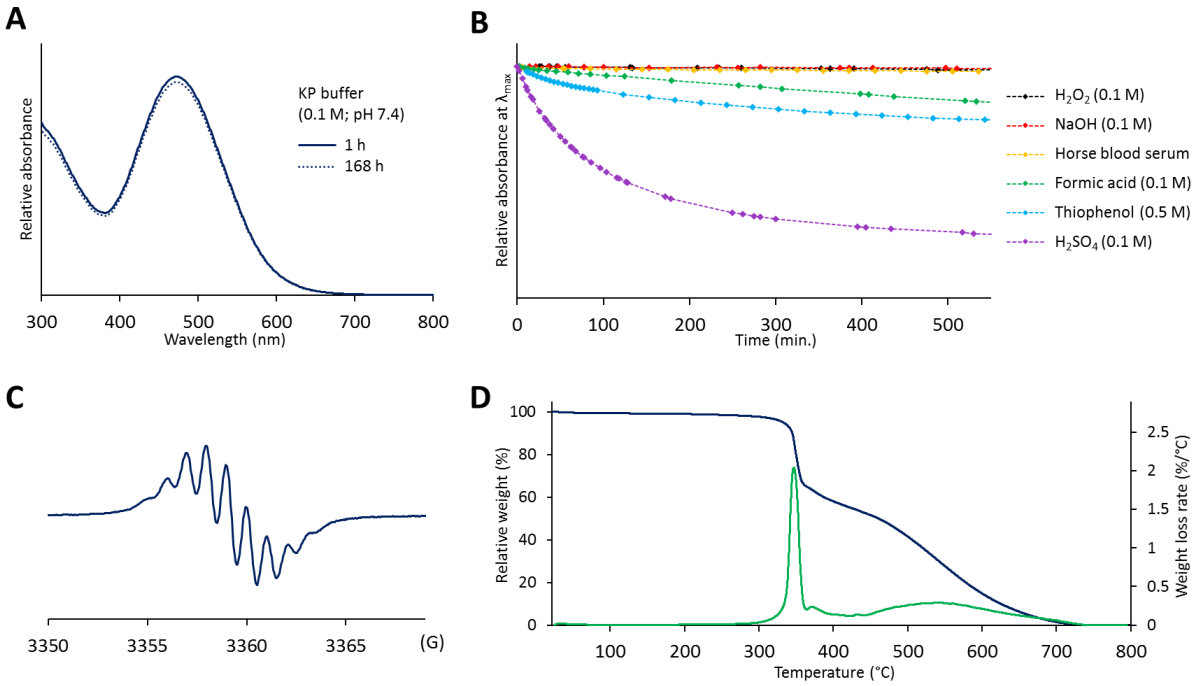

Figure 4. Stability of the 1,2-dicarbonyl radical.

(A) UV-vis spectra of 0.16 mM [**2a**$^{\bullet+}$][Cl$^-$] in potassium phosphate buffer (0.1 M, pH 7.4) 1 h (solid line) and 168 h (dotted line) after dissolution. λ_{max} = 472 nm.

(B) Decay of 0.16 mM [**2a**$^{\bullet+}$][Cl$^-$] in 0.1 M aqueous hydrogen peroxide (black, λ_{max} = 472 nm), 0.1 M aqueous sodium hydroxide (red, λ_{max} = 472 nm), horse blood serum (yellow, λ_{max} = 488 nm, serum(70%) mixed with distilled water(30%)), 0.1 M aqueous formic acid (green, λ_{max} = 472 nm), 0.5 M thiophenol in dichloromethane (blue, λ_{max} = 521 nm), and 0.1 M aqueous sulfuric acid (purple, λ_{max} = 472 nm).

(C) EPR spectra of [**2a**$^{\bullet+}$][Cl$^-$] after heating for 6 hours at 200 °C.

(D) Thermal gravimetric analysis (dark blue) and differential thermal gravimetric (DTG) analysis (green) of [**2a**$^{\bullet+}$][Cl$^-$] under air.

Thermal stability of [**2a**$^{\bullet+}$][Cl$^-$] was also measured by heating the solid sample up to 200 °C over 6 hours, which showed no sign of decomposition, color change, or phase transition. The EPR spectrum of the heated [**2a**$^{\bullet+}$][Cl$^-$] was identical to the spectrum of freshly synthesized sample (**Figure 4C**). Thermal gravimetric analysis (TGA) of [**2a**$^{\bullet+}$][Cl$^-$] under air showed decomposition temperature of *ca*. 300 °C (**Figure 4D**), which is among the highest decomposition temperature reported for organic radicals.[3]

Having highly stable and water soluble organic radical in hand, we considered the application of [**2a**$^{\bullet+}$][Cl$^-$] as an organic radical contrast agent for magnetic resonance imaging. Magnetic resonance imaging (MRI) is one of the most used biomedical imaging techniques;[16] however, toxicity of gadolinium based contrast agents restricts their use in some patients with impaired kidney performance.[17] Therefore, stable and water soluble organic radicals have been investigated as non-toxic alternative MRI contrast agents. Up to date, sterically hindered aminoxyl radicals show significant potential due to their accessibility and

functionalizability.[18] Although aminoxyl radicals show reasonable stability toward water, they rapidly decompose to hydroxylamines under physiological conditions due to reducing agents such as ascorbate.[19] For example, one of the most commonly used organic contrast agents, 3-carboxy-2,2,5,5-tetramethyl-1-pyrrolidinyloxy radical (3-CP) has a half-life of only ~2 minutes *in vivo*. Relaxation performance of [**2a**$^{\bullet+}$][Cl^-] was measured at the magnetic field of 7 T (**Figure S18**), which showed longitudinal (r_1 = 0.14 mM^{-1} s^{-1}) and transverse relaxivity (r_2 = 0.58 mM^{-1} s^{-1}) comparable to or higher than other organic molecule-based contrast agents (e.g. r_1 = 0.15 mM^{-1} s^{-1}, r_2 = 0.17 mM^{-1} s^{-1} for 3-CP).[20]

In summary, highly stable and water soluble 1,2-dicarbonyl radicals **2a**$^{\bullet+}$ and **2b**$^{\bullet+}$ were synthesized and fully characterized. X-ray crystallography, EPR spectroscopy, and DFT calculation suggest the unpaired electron is located on the central C_2O_2 unit, which is a rare example of NHC-derived radicals with minimal delocalization of spin density over the NHC fragments. In addition, **2a**$^{\bullet+}$ and **2b**$^{\bullet+}$ showed high stability towards various chemical and physiological conditions. Interestingly, similar longitudinal relaxivity and higher transverse relaxivity was observed compared to the previously reported organic molecule-based contrast agents which makes these radicals promising candidates for organic radical MRI contrast agents.

Acknowledgements

This work was supported by the National Supercomputing Center with supercomputing resources including technical support (KSC-2019-CRE-0162), and by the National Research Foundation of Korea (NRF-2019R1A2C2010732). X-ray diffraction experiment with synchrotron radiation was performed at the Pohang Accelerator Laboratory (Beamline 2D). High resolution mass spectrometry was performed at the Korea Basic Science Institute (DS107). We thank Dr. Younghoon Kim for assistance with TGA analysis, and Dr. Ewa Pietrasiak and Dr. Dmitry V. Yandulov for helpful discussions.

Author contributions

Y. K. designed and synthesized the 1,2-dicarbonyl radicals, performed experiments and characterization, and wrote the manuscript. J. E. B. assisted the synthesis of the radicals, and obtained experimental EPR spectrum of [**2a**$^{\bullet+}$][BF_4^-] and [**2b**$^{\bullet+}$][BF_4^-]. G. Y. J. measured the stability of [**2a**$^{\bullet+}$][Cl^-] in the buffer solutions. S. S. K. assisted the NMR relaxation experiments. H. S. measured the cyclic voltammograms. E. L. directed the project.

Notes

The authors declare the following competing financial interest: A patent application has been led through POSTECH on methods and reagents presented in this manuscript.

References

(1) Gomberg, M. An Instance of Trivalent Carbon: Triphenylmethyl. *J. Am. Chem. Soc.* **1900,** *22*, 757-771.

(2) (a) Forrester, A. R.; Thomson, R. H. Stable Nitroxide Radicals. *Nature* **1964,** *203*, 74-75. (b) Back, O.; Celik, M. A.; Frenking, G.; Melaimi, M.; Donnadieu, B.; Bertrand, G. A crystalline phosphinyl radical cation. *J. Am. Chem. Soc.* **2010,** *132*, 10262-10263.

(3) Hicks, R. G., *Stable Radicals: Fundamentals and Applied Aspects of Odd-Electron Compounds*. John Wiley & Sons, Ltd: 2010.

(4) (a) Xia, S.; Villamena, F. A.; Hadad, C. M.; Kuppusamy, P.; Li, Y.; Zhu, H.; Zweier, J. L. Reactivity of molecular oxygen with ethoxycarbonyl derivatives of tetrathiatriarylmethyl radicals. *J. Org. Chem.* **2006,** *71*, 7268-7279. (b) Frank, J.; Elewa, M.; Said, M. M.; El Shihawy, H. A.; El-Sadek, M.; Muller, D.; Meister, A.; Hause, G.; Drescher, S.; Metz, H.; Imming, P.; Mader, K. Synthesis, Characterization, and Nanoencapsulation of Tetrathiatriarylmethyl and Tetrachlorotriarylmethyl (Trityl) Radical Derivatives-A Study To Advance Their Applicability as in Vivo EPR Oxygen Sensors. *J. Org. Chem.* **2015,** *80*, 6754-6766. (c) Hintz, H.; Vanas, A.; Klose, D.; Jeschke, G.; Godt, A. Trityl Radicals with a Combination of the Orthogonal Functional Groups Ethyne and Carboxyl: Synthesis without a Statistical Step and EPR Characterization. *J. Org. Chem.* **2019,** *84*, 3304-3320.

(5) (a) Tomioka, H.; Iwamoto, E.; Itakura, H.; Hirai, K. Generation and characterization of a fairly stable triplet carbene. *Nature* **2001,** *412*, 626-628. (b) Tang, B.; Zhao, J.; Xu, J.-F.; Zhang, X. Tuning the stability of organic radicals: from covalent approaches to non-covalent approaches. *Chem. Sci.* **2020,** *11*, 1192-1204.

(6) Russell, G. A.; Strom, E. T.; Talaty, E. R.; Weiner, S. A. Semidiones. I. Acyclic Semidione Radical Anions and Cations Containing a Single Aryl Substituent1. *J. Am. Chem. Soc.* **1966,** *88*, 1998-2004.

(7) (a) Zanello, P.; Corsini, M. Homoleptic, mononuclear transition metal complexes of 1,2-dioxolenes: Updating their electrochemical-to-structural (X-ray) properties. *Coord. Chem. Rev.* **2006,** *250*, 2000-2022. (b) Kirk, M. L.; Shultz, D. A. Transition metal complexes of donor–acceptor biradicals. *Coord. Chem. Rev.* **2013,** *257*, 218-233.

(8) (a) Hopkinson, M. N.; Richter, C.; Schedler, M.; Glorius, F. An overview of N-heterocyclic carbenes. *Nature* **2014,** *510*, 485-496. (b) Bourissou, D.; Guerret, O.; Gabbaï, F. P.; Bertrand, G. Stable Carbenes. *Chem. Rev.* **2000,** *100*, 39-92. (c) Igau, A.; Grutzmacher, H.; Baceiredo, A.; Bertrand, G. Analogous α,α'-bis-carbenoid, triply bonded species: synthesis of a stable λ3-phosphino carbene-λ5-phosphaacetylene. *J. Am. Chem. Soc.* **1988,** *110*, 6463-6466. (d) Arduengo, A. J.; Harlow, R. L.; Kline, M. A stable crystalline carbene. *J. Am. Chem. Soc.* **1991,** *113*, 361-363. (e) Lavallo, V.; Canac, Y.; Prasang, C.; Donnadieu, B.; Bertrand, G. Stable cyclic (alkyl)(amino)carbenes as rigid or flexible, bulky,

electron-rich ligands for transition-metal catalysts: a quaternary carbon atom makes the difference. *Angew. Chem. Int. Ed.* **2005,** *44*, 5705-5709. (f) Melaimi, M.; Soleilhavoup, M.; Bertrand, G. Stable Cyclic Carbenes and Related Species beyond Diaminocarbenes. *Angew. Chem. Int. Ed.* **2010,** *49*, 8810-8849.

(9) (a) Wang, Y.; Robinson, G. H. Carbene-stabilized main group diatomic allotropes. *Dalton Trans.* **2012,** *41*, 337-345. (b) Chandra Mondal, K.; Roy, S.; Roesky, H. W. Silicon based radicals, radical ions, diradicals and diradicaloids. *Chem. Soc. Rev.* **2016,** *45*, 1080-1111. (c) Yao, S.; Xiong, Y.; Driess, M. A New Area in Main-Group Chemistry: Zerovalent Monoatomic Silicon Compounds and Their Analogues. *Acc. Chem. Res.* **2017,** *50*, 2026-2037.

(10) Martin, C. D.; Soleilhavoup, M.; Bertrand, G. Carbene-Stabilized Main Group Radicals and Radical Ions. *Chem. Sci.* **2013,** *4*, 3020-3030.

(11) (a) Mahoney, J. K.; Martin, D.; Moore, C. E.; Rheingold, A. L.; Bertrand, G. Bottleable (amino)(carboxy) radicals derived from cyclic (alkyl)(amino) carbenes. *J. Am. Chem. Soc.* **2013,** *135*, 18766-18769. (b) Martin, D.; Moore, C. E.; Rheingold, A. L.; Bertrand, G. An air-stable oxyallyl radical cation. *Angew. Chem. Int. Ed.* **2013,** *52*, 7014-7017. (c) Mahoney, J. K.; Martin, D.; Thomas, F.; Moore, C. E.; Rheingold, A. L.; Bertrand, G. Air-persistent monomeric (amino)(carboxy) radicals derived from cyclic (alkyl)(amino) carbenes. *J. Am. Chem. Soc.* **2015,** *137*, 7519-7525. (d) Deardorff, C. L.; Eric Sikma, R.; Rhodes, C. P.; Hudnall, T. W. Carbene-derived alpha-acyl formamidinium cations: organic molecules with readily tunable multiple redox processes. *Chem. Commun.* **2016,** *52*, 9024-9027. (e) Regnier, V.; Molton, F.; Philouze, C.; Martin, D. An air-persistent oxyallyl radical cation with simple di(methyl)amino substituents. *Chem. Commun.* **2016,** *52*, 11422-11425. (f) Mahoney, J. K.; Jazzar, R.; Royal, G.; Martin, D.; Bertrand, G. The Advantages of Cyclic Over Acyclic Carbenes To Access Isolable Capto-Dative C-Centered Radicals. *Chem. Eur. J.* **2017,** *23*, 6206-6212.

(12) (a) Hansmann, M. M.; Melaimi, M.; Bertrand, G. Crystalline Monomeric Allenyl/Propargyl Radical. *J. Am. Chem. Soc.* **2017,** *139*, 15620-15623. (b) Li, Y.; Mondal, K. C.; Samuel, P. P.; Zhu, H.; Orben, C. M.; Panneerselvam, S.; Dittrich, B.; Schwederski, B.; Kaim, W.; Mondal, T.; Koley, D.; Roesky, H. W. C4 cumulene and the corresponding air-stable radical cation and dication. *Angew. Chem. Int. Ed.* **2014,** *53*, 4168-4172. (c) Jin, L.; Melaimi, M.; Liu, L.; Bertrand, G. Singlet carbenes as mimics for transition metals: synthesis of an air stable organic mixed valence compound [M2(C2)+˙; M = cyclic(alkyl)(amino)carbene]. *Org. Chem. Front.* **2014,** *1*, 351-354. (d) Hansmann, M. M.; Melaimi, M.; Bertrand, G. Organic Mixed Valence Compounds Derived from Cyclic (Alkyl)(amino)carbenes. *J. Am. Chem. Soc.* **2018,** *140*, 2206-2213. (e) Hansmann, M. M.; Melaimi, M.; Munz, D.; Bertrand, G. Modular Approach to Kekule Diradicaloids Derived from Cyclic (Alkyl)(amino)carbenes. *J. Am. Chem. Soc.* **2018,** *140*, 2546-2554.

(13) (a) Eymann, L. Y. M.; Tskhovrebov, A. G.; Sienkiewicz, A.; Bila, J. L.; Zivkovic, I.; Ronnow, H. M.; Wodrich, M. D.; Vannay, L.; Corminboeuf, C.; Pattison, P.; Solari, E.; Scopelliti, R.; Severin, K. Neutral Aminyl Radicals Derived from Azoimidazolium Dyes. *J. Am. Chem. Soc.* **2016,** *138*, 15126-15129. (b) Back, J.; Park, J.; Kim, Y.; Kang, H.; Kim, Y.; Park, M. J.; Kim, K.; Lee, E. Triazenyl Radicals Stabilized by N-Heterocyclic Carbenes. *J. Am. Chem. Soc.* **2017,** *139*, 15300-15303.

(14) (a) Ueng, S. H.; Solovyev, A.; Yuan, X.; Geib, S. J.; Fensterbank, L.; Lacote, E.; Malacria, M.; Newcomb, M.; Walton, J. C.; Curran, D. P. N-heterocyclic carbene boryl radicals: a new class of boron-centered radical. *J. Am. Chem. Soc.* **2009,** *131*, 11256-11262. (b) Tanaka, H.; Ichinohe, M.; Sekiguchi, A. An isolable NHC-stabilized silylene radical cation: synthesis and structural characterization. *J. Am. Chem. Soc.* **2012,** *134*, 5540-5543. (c) Matsumoto, T.; Gabbaï, F. P. A Borenium Cation Stabilized by an N-Heterocyclic Carbene Ligand. *Organometallics* **2009,** *28*, 4252-4253. (d) Bissinger, P.; Braunschweig, H.; Damme, A.; Krummenacher, I.; Phukan, A. K.; Radacki, K.; Sugawara, S. Isolation of a neutral boron-containing radical stabilized by a cyclic (alkyl)(amino)carbene. *Angew. Chem. Int. Ed.* **2014,** *53*, 7360-7363. (e) Park, J.; Song, H.; Kim, Y.; Eun, B.; Kim, Y.; Bae, D. Y.; Park, S.; Rhee, Y. M.; Kim, W. J.; Kim, K.; Lee, E. N-heterocyclic carbene nitric oxide radicals. *J. Am. Chem. Soc.* **2015,** *137*, 4642-4645. (f) Abraham, M. Y.; Wang, Y.; Xie, Y.; Gilliard, R. J., Jr.; Wei, P.; Vaccaro, B. J.; Johnson, M. K.; Schaefer, H. F., 3rd; Schleyer, P. V.; Robinson, G. H. Oxidation of carbene-stabilized diarsenic: diarsene dications and diarsenic radical cations. *J. Am. Chem. Soc.* **2013,** *135*, 2486-2488. (g) Park, J. S.; Karnas, E.; Ohkubo, K.; Chen, P.; Kadish, K. M.; Fukuzumi, S.; Bielawski, C. W.; Hudnall, T. W.; Lynch, V. M.; Sessler, J. L. Ion-mediated electron transfer in a supramolecular donor-acceptor ensemble. *Science* **2010,** *329*, 1324-1327. (h) Silva Valverde, M. F.; Schweyen, P.; Gisinger, D.; Bannenberg, T.; Freytag, M.; Kleeberg, C.; Tamm, M. N-Heterocyclic Carbene Stabilized Boryl Radicals. *Angew. Chem. Int. Ed.* **2017,** *56*, 1135-1140. (i) Kim, Y.; Kim, K.; Lee, E. Oxime Ether Radical Cations Stabilized by N-Heterocyclic Carbenes. *Angew. Chem. Int. Ed.* **2018,** *57*, 262-265. (j) Li, B.; Kundu, S.; Stuckl, A. C.; Zhu, H.; Keil, H.; Herbst-Irmer, R.; Stalke, D.; Schwederski, B.; Kaim, W.; Andrada, D. M.; Frenking, G.; Roesky, H. W. A Stable Neutral Radical in the Coordination Sphere of Aluminum. *Angew. Chem. Int. Ed.* **2017,** *56*, 397-400. (k) Kim, Y.; Lee, E. An air-stable N-heterocyclic carbene iminoxyl borate radical zwitterion. *Chem. Commun.* **2018,** *54*, 6824-6827. (l) Sharma, M. K.; Blomeyer, S.; Glodde, T.; Neumann, B.; Stammler, H.-G.; Hinz, A.; van Gastel, M.; Ghadwal, R. S. Isolation of singlet carbene derived 2-phospha-1,3-butadienes and their sequential one-electron oxidation to radical cations and dications. *Chem. Sci.* **2020,** *11*, 1975-1984. (m) Styra, S.; Melaimi, M.; Moore, C. E.; Rheingold, A. L.; Augenstein, T.; Breher, F.; Bertrand, G. Crystalline Cyclic (Alkyl)(amino)carbene-tetrafluoropyridyl Radical. *Chem. Eur. J.* **2015,** *21*, 8441-8446. (n) Rottschafer, D.; Neumann, B.; Stammler, H. G.; van Gastel, M.; Andrada, D. M.; Ghadwal, R. S. Crystalline Radicals Derived from Classical N-Heterocyclic Carbenes. *Angew. Chem. Int. Ed.* **2018,** *57*, 4765-4768.

(15) Kim, Y.; Lee, E. Stable Organic Radicals Derived from N-Heterocyclic Carbenes. *Chem. Eur. J.* **2018,** *24*, 19110-19121.

(16) (a) Terreno, E.; Castelli, D. D.; Viale, A.; Aime, S. Challenges for molecular magnetic resonance imaging. *Chem. Rev.* **2010,** *110*, 3019-3042. (b) Caravan, P.; Ellison, J. J.; McMurry, T. J.; Lauffer, R. B. Gadolinium(III) Chelates as MRI Contrast Agents: Structure, Dynamics, and Applications. *Chem. Rev.* **1999,** *99*, 2293-2352.

(17) Olchowy, C.; Cebulski, K.; Lasecki, M.; Chaber, R.; Olchowy, A.; Kalwak, K.; Zaleska-Dorobisz, U. The presence of the gadolinium-based contrast agent depositions in the brain and symptoms of gadolinium neurotoxicity - A systematic review. *PLoS One* **2017,** *12*, e0171704.

(18) (a) Janzen, E. G.; Towner, R. A., Aminoxyl Radicals as MRI Contrast Agents. In *Bioactive Spin Labels*, Zhdanov, R. I., Ed. Springer Berlin Heidelberg: Berlin, Heidelberg, 1992; pp 573-583. (b) Sowers, M. A.; McCombs, J. R.; Wang, Y.; Paletta, J. T.; Morton, S. W.; Dreaden, E. C.; Boska, M. D.; Ottaviani, M. F.; Hammond, P. T.; Rajca, A.; Johnson, J. A. Redox-responsive branched-bottlebrush polymers for in vivo MRI and fluorescence imaging. *Nat Commun* **2014,** *5*, 5460.

(19) (a) Paletta, J. T.; Pink, M.; Foley, B.; Rajca, S.; Rajca, A. Synthesis and reduction kinetics of sterically shielded pyrrolidine nitroxides. *Org. Lett.* **2012,** *14*, 5322-5325. (b) Hyodo, F.; Matsumoto, K.; Matsumoto, A.; Mitchell, J. B.; Krishna, M. C. Probing the intracellular redox status of tumors with magnetic resonance imaging and redox-sensitive contrast agents. *Cancer Res.* **2006,** *66*, 9921-9928.

(20) (a) Rajca, A.; Wang, Y.; Boska, M.; Paletta, J. T.; Olankitwanit, A.; Swanson, M. A.; Mitchell, D. G.; Eaton, S. S.; Eaton, G. R.; Rajca, S. Organic radical contrast agents for magnetic resonance imaging. *J. Am. Chem. Soc.* **2012,** *134*, 15724-15727. (b) Nguyen, H. V.; Chen, Q.; Paletta, J. T.; Harvey, P.; Jiang, Y.; Zhang, H.; Boska, M. D.; Ottaviani, M. F.; Jasanoff, A.; Rajca, A.; Johnson, J. A. Nitroxide-Based Macromolecular Contrast Agents with Unprecedented Transverse Relaxivity and Stability for Magnetic Resonance Imaging of Tumors. *ACS Cent. Sci.* **2017,** *3*, 800-811.

Electronic Supplementary Information

1,2-Dicarbonyl Radicals with Exceptional Physiological and Chemical Stability

Youngsuk Kim,[a] Jung Eun Byeon,[a] Gu Yoon Jeong,[a] Seoungsu Kim,[a] Hayoung Song,[a] Eunsung Lee*[,a]

[a] Department of Chemistry, Pohang University of Science and Technology (POSTECH), Pohang, 37673, Republic of Korea

*E-mail: eslee@postech.ac.kr

Table of contents

Materials and Methods

1. General methods

All air- and moisture-insensitive reactions were carried out under an ambient atmosphere, magnetically stirred. All air- and moisture-sensitive manipulations were performed using oven-dried glassware, including standard Schlenk and glovebox techniques under an atmosphere of nitrogen. High resolution mass spectrometry was performed at the Korea Basic Science Institute with a JEOL JMS 700 high resolution mass spectrometer. Thermal gravimetric analyses (TGA) were performed under air with a Perkin Elmer Pyris 1. Elemental analyses were performed at Ulsan National Institute of Science and Technology (UNIST) Central Research Facilities with a Leco Truspec Micro elemental analyzer.

2. Reagents

IMes (**1a**), IDipp (**1b**), and $IMesH^+Cl^-$ were synthesized according to a reference.[1] Oxalyl chloride $(COCl)_2$ and all other chemicals were purchased from commercial sources and used as received unless otherwise specified. Horse blood serum was purchased from Sigma-Aldrich Korea (product No. H1138) and used as received. 3Å molecular sieves were activated at 240 ˚C under dynamic vacuum for overnight prior to use. Benzene, toluene, pentane, diethyl ether, and THF (tetrahydrofuran) was distilled from deep purple sodium benzophenone ketyl and stored over activated 3Å molecular sieves. Acetonitrile-d_3 (CD_3CN) was dried using activated 3Å molecular sieves.

Experimental Details

Synthesis of [2a$^{\bullet+}$][BF_4^-]

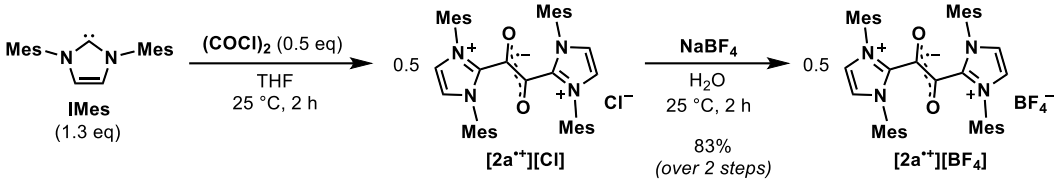

In a N_2 atmosphere glovebox, IMes (200 mg, 0.66 mmol, 1.3 eq) was placed in a 20 mL vial and subsequently dry THF (4 mL) was added to the vial. The solution was stirred at 25 °C, and dry THF solution (1 mL) of oxalyl chloride ($(COCl)_2$, 21.6 μL, 0.25 mmol, 0.5 eq) was slowly added. After 2 hours, the resulting precipitate was collected on a frit, washed with dry THF (3 × 3 mL) and dry diethyl ether (3 × 3 mL), and dried *in vacuo* to afford **[2a$^{\bullet+}$][Cl$^-$]** as a purple solid. The obtained **[2a$^{\bullet+}$][Cl$^-$]** was then suspended in distilled water (5 mL) and aqueous solution (1 mL) of sodium tetrafluoroborate ($NaBF_4$, 40 mg) was added. After 2 hours, the purple precipitate was collected on a frit, washed with distilled water (3 × 3 mL), and dried *in vacuo* to afford 158 mg of the product (83% over 2 steps). Single crystals of **[2a$^{\bullet+}$][Cl$^-$]** suitable for X-ray crystallography were obtained from slow evaporation of water/acetone mixture solution. Single crystals of **[2a$^{\bullet+}$][BF_4^-]** suitable for X-ray crystallography were obtained from slow diffusion of pentane into dichloromethane solution. Anal. Calcd for $C_{44}H_{48}BF_4N_4O_2$: C, 70.31; H, 6.44; N, 7.45. Found: C, 69.99; H, 7.01; N, 7.48. HRMS (FAB): m/z calcd for [$C_{44}H_{48}N_4O_2$ $(M)^+$] 664.3777, found 664.3779.

Synthesis of [2b$^{\bullet+}$][BF_4^-]

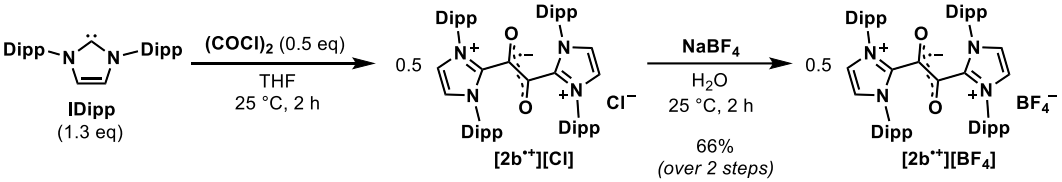

In a N_2 atmosphere glovebox, IDipp (100 mg, 0.26 mmol, 1.3 eq) was placed in a 20 mL vial and subsequently dry THF (2 mL) was added to the vial. The solution was stirred at 25 °C, and dry THF solution (1 mL) of oxalyl chloride ($(COCl)_2$, 8.4 μL, 0.10 mmol, 0.5 eq) was slowly added. After 2 hours, dry pentane (15 mL) was added, and the resulting precipitate was washed with diethyl ether (2 × 1 mL) and dried *in vacuo*. Further washing with distilled water (3 × 3 mL) afford **[2b$^{\bullet+}$][Cl$^-$]** as a purple solid. The obtained **[2b$^{\bullet+}$][Cl$^-$]** was then suspended in distilled water (1 mL) and aqueous solution (1 mL) of sodium tetrafluoroborate ($NaBF_4$, 15 mg) was added. After 2 hours, the purple precipitate was collected on a frit, washed with distilled water (3 × 3 mL), and dried *in vacuo* to afford 60.4 mg of the product (66% over 2 steps). Single crystals of **[2b$^{\bullet+}$][Cl$^-$]** suitable for X-ray crystallography were obtained from slow evaporation of water/acetone mixture solution. Anal. Calcd for $C_{56}H_{72}BF_4N_4O_2$: C, 73.11; H, 7.89; N, 6.09 (*cf.* $C_{56}H_{72}BF_4N_4O_2 \cdot 2H_2O$: C, 70.35; H, 8.01; N, 5.86). Found: C, 70.39; H, 8.35; N, 5.67. HRMS (FAB): m/z calcd for [$C_{56}H_{72}N_4O_2$ $(M)^+$] 832.5655, found 832.5658.

Synthesis of $[2a^{2+}][BF_4^-]_2$

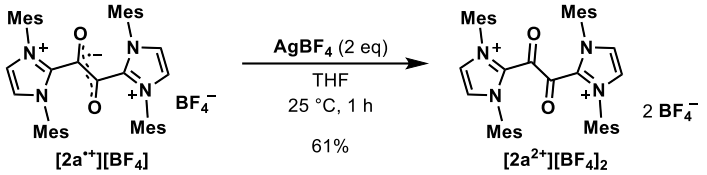

In a N_2 atmosphere glovebox, **$[2a^{\bullet+}][BF_4^-]$** (30 mg, 0.040 mmol) and silver(I) tetrafluoroborate ($AgBF_4$, 16 mg, 0.080 mmol, 2 eq) were placed in a 4 mL vial and subsequently dry THF (2 mL) was added to the vial. After 1 hour, the reaction mixture was centrifuged and decanted, and the remaining brown precipitate was dissolved in dry dichloromethane (3 mL). The solution was filtered through Celite to remove silver containing byproducts, and the filtrate was concentrated *in vacuo*. Dry pentane (3 mL) was added and the resulting precipitate was washed with dry THF (1 × 1 mL) and dry pentane (2 × 1 mL), and dried *in vacuo* to afford **$[2a^{2+}][BF_4^-]_2$** as an orange solid. (20 mg, 61%). ^{1}H NMR (500 MHz, Acetonitrile-d_3) δ 7.97 (s, 4H), 7.10 (s, 8H), 2.44 (s, 12H), 1.72 (s, 24H) ppm. ^{13}C{^{1}H} NMR (126 MHz, Acetonitrile-d_3) δ 172.4, 144.1, 135.6, 135.4, 131.3, 130.5, 129.6, 21.3, 17.2 ppm. ^{19}F{^{1}H} NMR (470 MHz, Acetonitrile-d_3) δ –151.8 ppm. Single crystals of **$[2a^{2+}][BF_4^-]_2$** suitable for X-ray crystallography were obtained from dichloromethane/pentane solution. Anal. Calcd for $C_{44}H_{48}B_2F_8N_4O_2$: C, 63.03; H, 5.77 (*cf.* $C_{44}H_{48}B_2F_8N_4O_2 \cdot H_2O$: C, 61.70; H, 5.88; N, 6.54); N, 6.68. Found: C, 61.54; H, 6.24; N, 6.73.

Mechanistic study

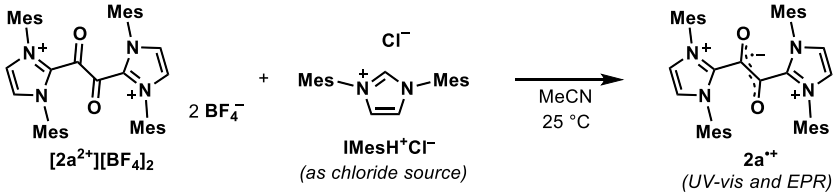

We proposed that the formation of **$2a^{\bullet+}$** from IMes and oxalyl chloride involves the formation of **$2a^{2+}$** as an intermediate followed by a spontaneous one electron reduction. Interestingly, the reaction does not require additional reducing agent, therefore chloride or NHC in the reaction mixture may act as electron source. (Single electron transfer from NHCs to electron acceptors have been recently reported by Severin and co-workers.[2]) Indeed, the reaction between **$[2a^{2+}][BF_4^-]_2$** with $IMesH^+Cl^-$ (as a soluble chloride source) afforded **$2a^{\bullet+}$** which was detected by EPR (**Figure S6**) and UV-vis spectroscopy (**Figure S14**).

DFT Calculation

General information

Geometry optimizations and frequency calculations were performed using Gaussian16[3] with M06-2X functional[4] and Def2-SVP basis set.[5] In the geometry optimization, the default tight convergence in the SCF cycle was used without any orbital symmetry constraints. Multiwfn[6] and IBOview[7, 8] programs were used to visualize Molecular orbitals. Wiberg bond indices (WBIs) were calculated from the optimized geometry with Löwdin orthogonalization method using Multiwfn.

Coordinates of optimized structures

The following optimized geometries were displayed in Cartesian coordinates (atomic unit). E° represents the electronic energy of the optimized structure, and G° represents the sum of electronic and thermal free energies in Hartree unit.

2a$^{\bullet+}$ [E° = –2071.7768846; G° = –2071.044877]

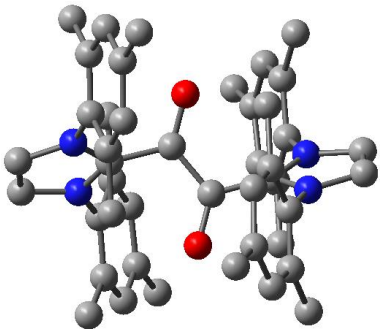

Charge = 1; Multiplicity = 2;

	Atomic coordinates (Cartesian; in atomic unit)			Mulliken charge	Spin density
O	-0.0171840011	0.8480612757	1.5432186703	-0.276975	0.322261
N	0.9531572985	2.2329742473	-1.4784521889	-0.177772	0.009341
N	-0.9732981757	2.7149840828	-0.6067925669	-0.181867	0.010149
C	2.4091076556	0.9420679413	-2.9519629225	0.086987	0.001577
C	2.2240605153	1.6070448015	-1.7292426389	-0.033928	-0.006434
C	0.0674792475	0.6436473770	0.3141463414	0.057964	0.179057
C	0.0239353394	1.8160944269	-0.6057497206	0.211481	-0.013777
C	3.6594787054	0.3698623447	-3.1785927654	-0.267071	0.003125
C	4.4690840987	1.1616235332	-1.0586920815	-0.242914	0.003365
C	3.2287593904	1.7339466230	-0.7630879147	0.085223	0.001990
C	4.7009967215	0.4707424115	-2.2484056471	0.107455	0.000364
C	0.5381273926	3.4256784095	-2.0427983886	0.012016	0.003733
C	-2.2305941130	2.5600911385	0.0775994805	-0.043861	-0.008295
C	-2.3963838824	3.1573589226	1.3315699438	0.105454	0.000265
C	-3.2298121400	1.8136799597	-0.5628971253	0.088162	0.003793
C	1.3143751224	0.8558351169	-3.9700781496	-0.278345	0.000132
C	-0.6723327553	3.7241587113	-1.5004434161	0.013144	0.000767
C	2.9946659818	2.4244000795	0.5467265236	-0.294230	-0.000158
C	6.0273876254	-0.1670551985	-2.5274792053	-0.291789	-0.000059
C	-4.6760882124	2.2816219918	1.3497569549	0.122873	-0.001051
C	-4.4536717854	1.7015103860	0.0963008306	-0.268962	0.002714
C	-2.9850936263	1.1408374659	-1.8800608933	-0.298792	0.001719
C	-3.6370766596	2.9965040076	1.9520802272	-0.264024	0.002089
C	-1.2722244549	3.8971478463	1.9866562079	-0.288616	0.000063
C	-6.0083484105	2.1367095349	2.0191393656	-0.293721	0.000045
O	0.0450386338	-0.8532861446	-1.5451881478	-0.274910	0.317473

N	0.9682139312	-2.2346430762	1.4780615542	-0.178061	0.008064
N	-0.9645257917	-2.7055824915	0.6155195095	-0.181705	0.008586
C	2.4261572893	-0.9418372919	2.9474275757	0.085212	0.001568
C	2.2414972536	-1.6128206725	1.7277742437	-0.035259	-0.005856
C	0.0887147157	-0.6426759186	-0.3160563645	0.060895	0.174180
C	0.0383976666	-1.8137499237	0.6085238373	0.212034	-0.013737
C	3.6783486717	-0.3737196800	3.1741596320	-0.266952	0.002665
C	4.4901718635	-1.1813863376	1.0609090934	-0.244279	0.002927
C	3.2482470968	-1.7502256497	0.7652188719	0.086841	0.001617
C	4.7217101734	-0.4842579349	2.2470516488	0.107347	0.000506
C	0.5477861985	-3.4233912138	2.0468923757	0.012035	0.003265
C	-2.2196681515	-2.5501033664	-0.0728717905	-0.045460	-0.007569
C	-2.3792667095	-3.1459445462	-1.3285783608	0.104887	0.000113
C	-3.2228628894	-1.8067274646	0.5650823993	0.088059	0.003239
C	1.3277353953	-0.8438509937	3.9607146171	-0.279997	0.000243
C	-0.6666785984	-3.7151261959	1.5100236738	0.013084	0.000432
C	3.0137801473	-2.4463548319	-0.5413489036	-0.294767	0.000190
C	6.0492842031	0.1516004232	2.5247718984	-0.291574	-0.000064
C	-4.6607342504	-2.2751666286	-1.3540590849	0.122729	-0.001094
C	-4.4443003572	-1.6962746954	-0.0989784656	-0.268678	0.002873
C	-2.9851946875	-1.1351507506	1.8840796445	-0.300387	0.001773
C	-3.6178478324	-2.9866973595	-1.9537064162	-0.263966	0.002218
C	-1.2512251705	-3.8833086432	-1.9800346042	-0.289807	0.000106
C	-5.9910309405	-2.1332838554	-2.0279831065	-0.293847	0.000045
H	3.8317012147	-0.1654768586	-4.1221151064	0.070696	-0.000165
H	5.2824065994	1.2628719938	-0.3276848581	0.055156	-0.000145
H	1.1582939485	3.9516630015	-2.7685913803	0.148413	-0.000102
H	0.3650257985	0.5334715365	-3.5048046940	0.155291	-0.001472
H	1.5713978993	0.1288258259	-4.7589619131	0.131561	0.000030
H	1.1388005612	1.8282621336	-4.4710468634	0.134084	0.000267
H	-1.3590170283	4.5547008771	-1.6656395769	0.148673	0.000160
H	2.3399054669	3.3121660621	0.4497993634	0.123237	0.000351
H	3.9492546739	2.7583575514	0.9899797818	0.137414	0.000098
H	2.5119923612	1.7453003246	1.2803583564	0.178205	-0.002899
H	5.9434354543	-1.2716775135	-2.5420020339	0.142645	0.000036
H	6.7818766630	0.1028438816	-1.7673387793	0.128512	-0.000002
H	6.4214581411	0.1313432420	-3.5166129787	0.149157	0.000022
H	-5.2648045298	1.1437080324	-0.3913640467	0.056835	-0.000148
H	-2.5821577851	1.8380279520	-2.6409819950	0.133316	0.000209
H	-3.9193244949	0.7101806190	-2.2807079016	0.132498	0.000126
H	-2.2546236949	0.3090113819	-1.7900628757	0.173171	-0.004960
H	-3.7948824908	3.4466638132	2.9408577139	0.070789	-0.000099
H	-0.4175994978	3.2124856766	2.1572794469	0.159792	-0.001657
H	-1.5829656261	4.3122489858	2.9600787092	0.131167	-0.000003
H	-0.9092277590	4.7390517369	1.3654504647	0.129980	-0.000009
H	-6.7652338221	2.7934029938	1.5483151435	0.153500	-0.000033
H	-5.9624728469	2.4027326059	3.0893594565	0.133675	-0.000004
H	-6.3907559489	1.1014627539	1.9378911605	0.133179	-0.000018
H	3.8503194711	0.1666981240	4.1148385297	0.070891	-0.000144
H	5.3047999237	-1.2892980079	0.3322310723	0.056081	-0.000118
H	1.1671362983	-3.9512315958	2.7720554134	0.148491	-0.000066
H	0.3824224081	-0.5163238818	3.4903323542	0.157241	-0.001677
H	1.5869475947	-0.1161534696	4.7482510592	0.131517	0.000024
H	1.1429291053	-1.8132832466	4.4641594120	0.134200	0.000299
H	-1.3579454475	-4.5410615212	1.6791221961	0.148758	0.000180
H	2.3544107279	-3.3303196345	-0.4411274991	0.123134	0.000304
H	3.9676266549	-2.7873201826	-0.9807433443	0.137352	0.000074
H	2.5351253701	-1.7687758814	-1.2790313149	0.178392	-0.002769
H	5.9672830290	1.2564271204	2.5355810917	0.142702	0.000040
H	6.8035153568	-0.1221056541	1.7657572082	0.128572	-0.000001
H	6.4423589001	-0.1443211695	3.5150535168	0.149333	0.000026
H	-5.2584021946	-1.1407521846	0.3863361519	0.056907	-0.000154
H	-2.5832789483	-1.8323578259	2.6455216867	0.132888	0.000181
H	-3.9224275095	-0.7079294588	2.2814253008	0.131950	0.000103
H	-2.2561490394	-0.3016188725	1.7982068532	0.175440	-0.004527
H	-3.7709799198	-3.4359122512	-2.9436478978	0.070847	-0.000109

H	-0.3967774988	-3.1974242456	-2.1474080548	0.161032	-0.001722
H	-1.5579122551	-4.2985835004	-2.9546713922	0.131215	-0.000004
H	-0.8893112421	-4.7249477061	-1.3577772067	0.130087	-0.000003
H	-6.7460036247	-2.7973811929	-1.5644968419	0.153709	-0.000034
H	-5.9393347552	-2.3923445976	-3.0996591041	0.133706	-0.000004
H	-6.3798044011	-1.1008649674	-1.9416280357	0.133241	-0.000018

2a^{2+} [E° = –2071.4621977; G° = –2070.733418]

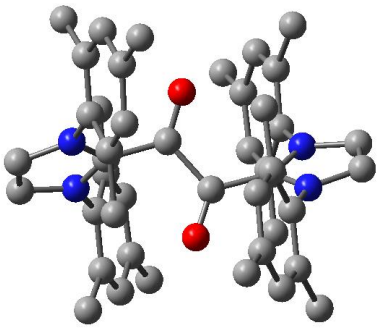

Charge = 2; Multiplicity = 1;

Atomic coordinates (Cartesian; in atomic unit)

O	-0.1905393215	0.7807802425	1.4919768034
N	0.9120797792	2.2614998348	-1.480069668
N	-1.0021782435	2.7656224305	-0.5660578252
C	2.3696970861	0.9921641829	-2.9749774886
C	2.1818919444	1.6232572344	-1.7327683588
C	0.0341725764	0.6803383683	0.3145461917
C	-0.0055729663	1.8656302091	-0.588111266
C	3.617705931	0.4171417241	-3.2034364553
C	4.4231277602	1.1645734566	-1.0634889168
C	3.1853084843	1.7375931435	-0.7599728726
C	4.6581545826	0.4965140755	-2.2664915457
C	0.4967764107	3.4488348839	-2.0335305503
C	-2.2680060412	2.611016062	0.1179985062
C	-2.4569018524	3.2662171024	1.3420600272
C	-3.2486108548	1.8265403976	-0.5065625783
C	1.2993956902	0.9607124522	-4.0229600819
C	-0.711846264	3.7553211504	-1.4715922955
C	2.9708053602	2.4375601104	0.5499493392
C	5.9887796129	-0.118579606	-2.5650706671
C	-4.7186463735	2.3374603259	1.3799794883
C	-4.4746951925	1.7159902535	0.1506671472
C	-3.0000546394	1.0989043486	-1.7954031644
C	-3.6967847336	3.0997196251	1.9591253493
C	-1.3744916151	4.0981141047	1.9575642164
C	-6.0517900204	2.2069273578	2.0460163471
O	0.1089312485	-0.8331864975	-1.5302097138
N	1.0170639204	-2.2642671167	1.4757156374
N	-0.9054292239	-2.7647279118	0.582111558
C	2.4491673635	-0.9496199183	2.9548443589
C	2.2818954777	-1.6145222168	1.7262148096
C	0.150101779	-0.6979520629	-0.3378190213
C	0.0964265439	-1.8747341842	0.5878662317
C	3.6912650618	-0.3645041683	3.1884132268
C	4.5321601542	-1.164746048	1.0813661214
C	3.3017185358	-1.7505612928	0.7732437475
C	4.7466166812	-0.4654584004	2.2704223253
C	0.5978039607	-3.4453438174	2.0465731705
C	-2.1664023936	-2.6118756605	-0.111297417
C	-2.3294245736	-3.2451926897	-1.351483905
C	-3.1775218445	-1.875481881	0.5259932293
C	1.3596595661	-0.8936018763	3.9823514038
C	-0.6138246963	-3.7510035117	1.4956031062
C	3.1116601687	-2.4750150097	-0.5259109181
C	6.0731703516	0.1550037705	2.5757059491
C	-4.6153078403	-2.3789246373	-1.3887741769
C	-4.4007072622	-1.786215769	-0.1400828632
C	-2.9792602531	-1.1834784513	1.8423827416
C	-3.5682112462	-3.0982879139	-1.9765180602
C	-1.2255341934	-4.0453916547	-1.9712798036
C	-5.9353519944	-2.2295393728	-2.077383503
H	3.795304018	-0.0948135551	-4.1585638751
H	5.2377824306	1.2610670765	-0.3340385313
H	1.1087437445	3.9762087597	-2.7666175507
H	0.2934175732	0.7952331973	-3.5964951615
H	1.4910463578	0.158123986	-4.7547661652
H	1.2680299017	1.9084021574	-4.5960044332
H	-1.4014683607	4.5833720159	-1.6434178505
H	2.2787163279	3.2982036719	0.4728686729
H	3.9271593845	2.8243849583	0.9429350705
H	2.5705125485	1.7520872507	1.3266343693
H	5.8948363457	-1.2053634289	-2.7533502056
H	6.7072278195	0.0272778782	-1.7398068817
H	6.4351269684	0.3184518152	-3.4778617178
H	-5.2728811938	1.1285711101	-0.3231177166
H	-2.321545076	1.6411950935	-2.4820357818
H	-3.9470815226	0.9281702913	-2.3367142479
H	-2.562568527	0.0925644488	-1.6201584217
H	-3.8748613503	3.5907227908	2.9243945358
H	-0.4423356438	3.5165235333	2.0974608455
H	-1.6812894189	4.4776699335	2.9459809297
H	-1.1249112723	4.9792693068	1.3348442058
H	-6.7603135712	2.9636257063	1.6566934807
H	-5.9833481663	2.3597669412	3.1367556681
H	-6.5068558457	1.2172613798	1.8592909712
H	3.8518413516	0.1738810949	4.1319491494
H	5.3569520646	-1.2718303378	0.3642857759
H	1.2109080757	-3.9658633107	2.7835492802
H	0.362796275	-0.7231358841	3.5357274003
H	1.5471452714	-0.0855078227	4.7091306478
H	1.3063287607	-1.8346439314	4.5646469517
H	-1.3062848188	-4.5746203335	1.6766343942
H	2.3708499154	-3.2948792216	-0.4642658655
H	4.063431273	-2.922013509	-0.8623822922
H	2.7853670829	-1.7866731273	-1.3340531162
H	5.965192326	1.2185632762	2.8605454254

H	6.7668631486	0.0929569897	1.7191303306	H	-0.313088532	-3.4354692238	-2.1173030739
H	6.559727333	-0.3498306988	3.4318388742	H	-1.5263514806	-4.4358371801	-2.9572708869
H	-5.2242220807	-1.2464010278	0.3476185428	H	-0.9463358607	-4.9169203196	-1.3476392023
H	-2.2200028706	-1.6654714763	2.4871289953	H	-6.775766233	-2.3876930565	-1.3777875236
H	-3.9251997998	-1.1544149255	2.4118497102	H	-6.0477950813	-2.9387657397	-2.9146013614
H	-2.6708363829	-0.1261599197	1.7016172366	H	-6.051947409	-1.2088039895	-2.4929074661
H	-3.7271801915	-3.5796658222	-2.9497900516				

Molecular orbitals

Figure S1. SOMO and LUMO of $\mathbf{2a}^{\bullet+}$.

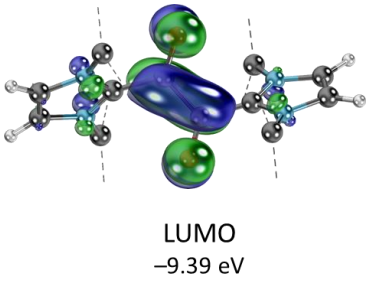

Figure S2. LUMO of $\mathbf{2a}^{2+}$.

Wiberg bond index

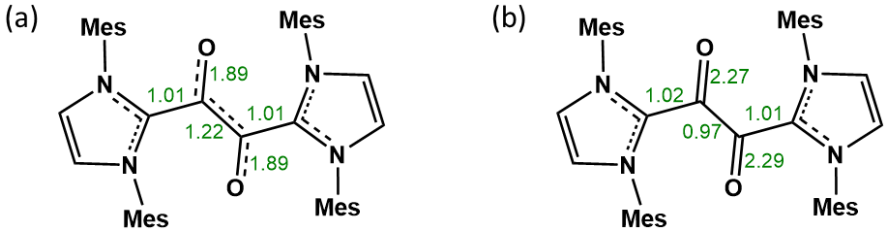

Figure S3. Selected Wiberg bond indices for (a) $\mathbf{2a}^{\bullet+}$ and (b) $\mathbf{2a}^{2+}$.

X-ray Crystallography

CCDC 2011174-2011177 contains the supplementary crystallographic data for [**2a**$^{\bullet+}$][BF_4^-], [**2b**$^{\bullet+}$][BF_4^-], [**2a**$^{2+}$][BF_4^-]$_2$, and [**2a**$^{\bullet+}$][Cl^-], respectively. These data can be obtained free of charge *via* https://www.ccdc.cam.ac.uk/

General information

A suitable crystal was coated with paratone-*N* oil and the diffraction data measured either with a graphite-monochromated Mo Kα radiation source on a Bruker Venture CMOS diffractometer or a synchrotron radiation on a 2D beamline at the Pohang Accelerator Laboratory, Korea. Using Olex2,[9] The structure was solved by ShelXT[10] using intrinsic phasing and refined by ShelXL[11] using least squares minimization. All the non-hydrogen atoms were refined anisotropically. All hydrogen atoms were added to their geometrically ideal positions. Solvent mask[12] was used to exclude solvent and some anion molecules during the refinement of [**2a**$^{\bullet+}$][Cl^-] (Grid = 0.25 Å, Solvent R = 1.2 Å).

	[**2a**$^{\bullet+}$][BF_4^-]	[**2b**$^{\bullet+}$][BF_4^-]	[**2a**$^{2+}$][BF_4^-]$_2$	[**2a**$^{\bullet+}$][Cl^-]
Empirical formula	$C_{44}H_{48}BF_4N_4O_2$	$C_{56}H_{72}BF_4N_4O_2$	$C_{46}H_{52}B_2Cl_4F_8N_4O_2$	$C_{44}H_{48}Cl_{0.67}N_4O_2$
Formula weight	751.67	919.98	1008.33	688.49
Temperature/K	100	100	100	100
Crystal system	monoclinic	monoclinic	monoclinic	trigonal
Space group	C2/c	$P2_1/n$	P-1	P-3c1
a/Å	19.1759(10)	14.6496(10)	11.438(7)	20.645(3)
b/Å	16.1466(10)	22.7009(14)	11.822(6)	20.645(3)
c/Å	15.4206(9)	16.5084(11)	20.180(12)	16.312(3)
α/°	90	90	88.103(15)	90
β/°	121.874(4)	92.586(2)	84.082(18)	90
γ/°	90	90	69.483(14)	120
Volume/Å^3	4054.7(4)	5484.4(6)	2542(3)	6021(2)
Z	4	4	2	6
ρ_{calc}g/cm^3	1.231	1.114	1.317	1.139
μ/mm^{-1}	0.088	0.076	0.302	0.111
F(000)	1588.0	1972.0	1044.0	2204.0
Crystal size/mm^3	0.15 × 0.08 × 0.05	0.3 × 0.05 × 0.05	0.3 × 0.15 × 0.03	0.08 × 0.04 × 0.03
Radiation	MoKα (λ = 0.71073)	MoKα (λ = 0.71073)	MoKα (λ = 0.71073)	Synchrotron (λ = 0.700)
2Θ range for data collection/°	3.752 to 52.178	4.356 to 50.066	4.146 to 50.054	3.886 to 59.632
Index ranges	$-23 \le h \le 23$ $-19 \le k \le 19$ $-19 \le l \le 19$	$-17 \le h \le 17$ $-27 \le k \le 27$ $-19 \le l \le 19$	$-13 \le h \le 13$ $-14 \le k \le 13$ $-24 \le l \le 24$	$-29 \le h \le 29$ $-24 \le k \le 24$ $-20 \le l \le 17$
Reflections collected	33905	84736	31410	15034
Independent reflections	3996 [R_{int} = 0.0645, R_{sigma} = 0.0298]	9692 [R_{int} = 0.1212, R_{sigma} = 0.0607]	8931 [R_{int} = 0.0963, R_{sigma} = 0.0906]	4642 [R_{int} = 0.0421, R_{sigma} = 0.0458]
Data/restraints/parameters	3996/0/255	9692/0/637	8931/78/668	4642/0/235
Goodness-of-fit on F^2	1.098	1.026	1.022	1.102
Final R indexes [I>=2σ (I)]	R_1 = 0.0565 wR_2 = 0.1585	R_1 = 0.0924 wR_2 = 0.2498	R_1 = 0.0808 wR_2 = 0.1936	R_1 = 0.0596 wR_2 = 0.1618
Final R indexes [all data]	R_1 = 0.0848 wR_2 = 0.1898	R_1 = 0.1639 wR_2 = 0.3088	R_1 = 0.1462 wR_2 = 0.2400	R_1 = 0.0815 wR_2 = 0.1725
Largest diff. peak/hole / e Å^{-3}	0.30/-0.24	0.52/-0.35	0.44/-0.45	0.36/-0.62

Structural data

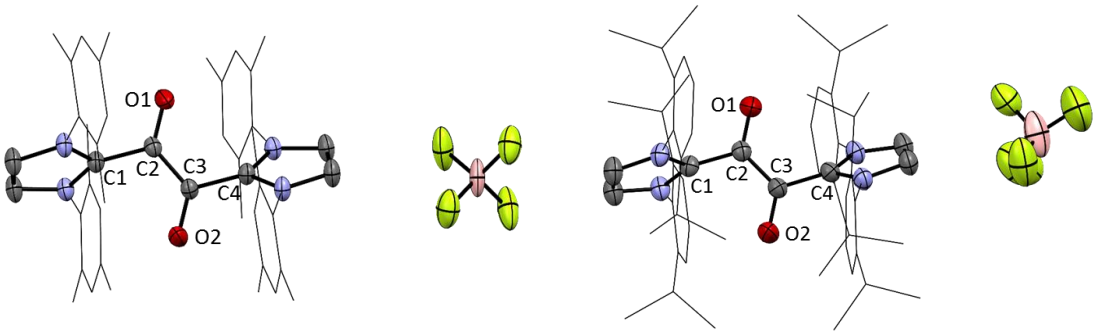

[**2a**$^{\bullet+}$][BF_4^-] [**2b**$^{\bullet+}$][BF_4^-]

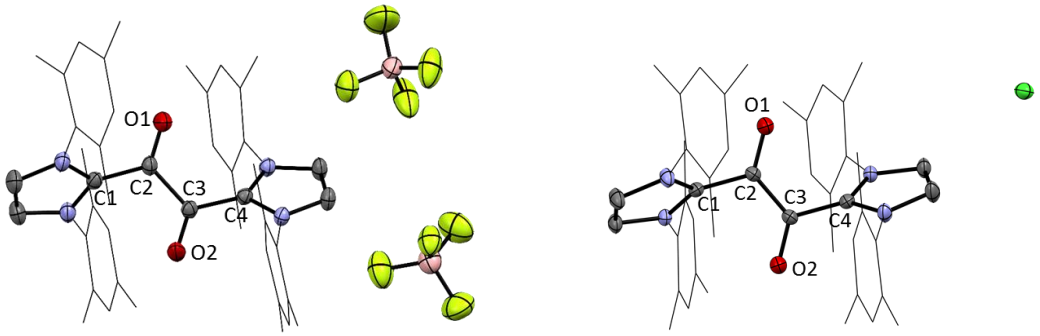

[**2a**$^{2+}$][BF_4^-]$_2$ [**2a**$^{\bullet+}$][Cl^-]

Table S1. Selected bond lengths (Å) and angles (°).

Bond length (Å)	C1–C2	C2–C3	C3–C4	O1–C2	O2–C3
[**2a**$^{\bullet+}$][BF_4^-]	1.495(3)	1.411(4)	1.495(3)	1.245(2)	1.245(2)
[**2b**$^{\bullet+}$][BF_4^-]	1.490(5)	1.406(4)	1.498(5)	1.245(4)	1.250(4)
[**2a**$^{2+}$][BF_4^-]$_2$	1.487(5)	1.536(5)	1.484(5)	1.192(5)	1.200(5)
[**2a**$^{\bullet+}$][Cl^-]	1.498(2)	1.433(3)	1.498(2)	1.249(3)	1.249(3)

Bond angle (°)	C1–C2–O1	O1–C2–C3	C1–C2–C3	C2–C3–O2	C2–C3–C4	O2–C3–C4
[**2a**$^{\bullet+}$][BF_4^-]	118.2(2)	125.1(2)	116.5(2)	125.1(2)	116.5(2)	118.2(2)
[**2b**$^{\bullet+}$][BF_4^-]	118.1(3)	123.5(3)	118.3(3)	123.6(3)	117.9(3)	118.4(3)
[**2a**$^{2+}$][BF_4^-]$_2$	121.3(4)	120.7(4)	117.3(3)	119.1(4)	119.1(3)	121.0(4)
[**2a**$^{\bullet+}$][Cl^-]	119.3(2)	125.2(2)	115.3(2)	125.2(2)	115.3(2)	119.3(2)

Torsion angle (°)	NHC–C1–C2–O1	O1–C2–C3–O2	O2–C3–C4–NHC2
[**2a**$^{\bullet+}$][BF_4^-]	53.0(3)	172.8(3)	53.0(3)
[**2b**$^{\bullet+}$][BF_4^-]	66.9(5)	179.3(4)	60.3(5)
[**2a**$^{2+}$][BF_4^-]$_2$	45.1(6)	156.8(4)	36.5(6)
[**2a**$^{\bullet+}$][Cl^-]	57.8(3)	171.0(2)	57.8(3)

The thermal ellipsoids are set at a 30% probability level except for [**2a**$^{\bullet+}$][Cl^-] (50% probability level). Hydrogens, solvents, disorders were omitted for clarity.

Table S2. Metric comparison between DFT optimized and X-ray determined structures.

Bond length (Å)	C1–C2	C2–C3	C3–C4	O1–C2	O2–C3
[**2a**$^{\bullet+}$][BF_4^-] (X-ray)	1.495(3)	1.411(4)	1.495(3)	1.245(2)	1.245(2)
2a$^{\bullet+}$ (DFT)	1.493	1.433	1.491	1.248	1.249
[**2a**$^{2+}$][BF_4^-]$_2$(X-ray)	1.487(5)	1.536(5)	1.484(5)	1.192(5)	1.200(5)
2a^{2+} (DFT)	1.498	1.529	1.490	1.201	1.203

Bond angle (°)	C1–C2–O1	O1–C2–C3	C1–C2–C3	C2–C3–O2	C2–C3–C4	O2–C3–C4
[**2a**$^{\bullet+}$][BF_4^-] (X-ray)	118.2(2)	125.1(2)	116.5(2)	125.1(2)	116.5(2)	118.2(2)
2a$^{\bullet+}$ (DFT)	118.5	125.8	115.6	125.5	115.8	118.5
[**2a**$^{2+}$][BF_4^-]$_2$(X-ray)	121.3(4)	120.7(4)	117.3(3)	119.1(4)	119.1(3)	121.0(4)
2a^{2+} (DFT)	121.6	121.5	116.2	120.5	117.4	121.4

Torsion angle (°)	NHC–C1–C2–O1	O1–C2–C3–O2	O2–C3–C4–NHC2
[**2a**$^{\bullet+}$][BF_4^-] (X-ray)	53.0(3)	172.8(3)	53.0(3)
2a$^{\bullet+}$ (DFT)	57.5	172.7	55.1
[**2a**$^{2+}$][BF_4^-]$_2$(X-ray)	45.1(6)	156.8(4)	36.5(6)
2a^{2+} (DFT)	56.8	165.1	46.5

DFT calculation at M06/Def2SV(P).

EPR

General information

EPR spectra were recorded on a Bruker X-band A200 spectrometer using dry dichloromethane solutions. Spectra processing and simulation were performed with Bruker WIN-EPR and EasySpin associated with DFT calculations.[13] Isotropic hyperfine coupling constants were initially computed using gaussian09 with M06/Def2-SV(P) basis sets, and then rescaled to fit the experimental data.

EPR spectra

(a)

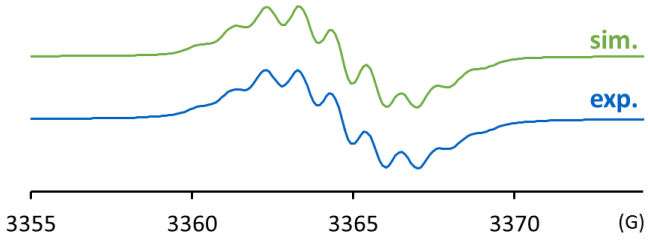

(b)

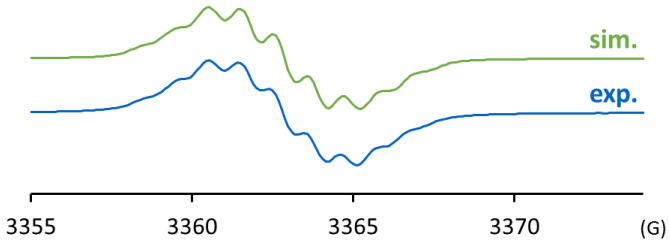

Figure S4. (a) Experimental (bottom, blue) and simulated (top, green) EPR spectra of **[2a$^{\bullet+}$][BF$_4^-$]** at microwave frequency = 9.4467 GHz. Simulated with the following parameters: g_{iso} = 2.0060; hyperfine coupling constants: $a(^{14}N)$ = 3.0, 3.0, 2.6, 2.6 MHz; Gaussian line width = 0.04 mT; Lorentzian line width = 0.04 mT. (b) Experimental (bottom, blue) and simulated (top, green) EPR spectra of **[2b$^{\bullet+}$][BF$_4^-$]** at microwave frequency = 9.4413 GHz. Simulated with the following parameters: g_{iso} = 2.0059; hyperfine coupling constants: $a(^{14}N)$ = 3.0, 3.0, 2.6, 2.6 MHz; Gaussian line width = 0.05 mT; Lorentzian line width = 0.04 mT.

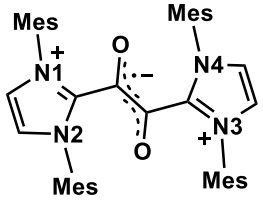

hfcc	N1	N2	N3	N4
Exp	2.6	3.0	2.6	3.0
DFT	3.7	4.5	3.6	4.4

Figure S5. Comparison of hyperfine coupling constants for **[2a$^{\bullet+}$][BF$_4^-$]** from experiment and DFT calculations at M06/Def2-SV(P).

Mechanistic study

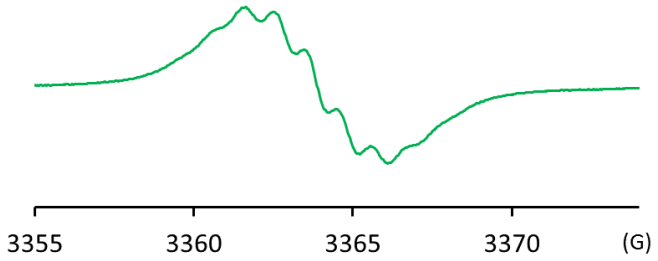

Figure S6. Experimental EPR spectra of the reaction mixture from the reaction between **[2a^{2+}][BF$_4^-$]$_2$** and IMesH$^+$Cl$^-$ at microwave frequency = 9.4452 GHz.

Thermal stability

a)

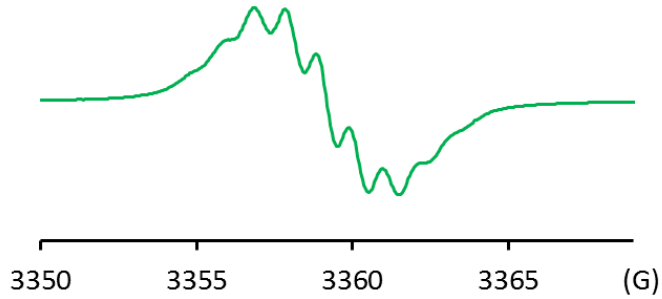

b)

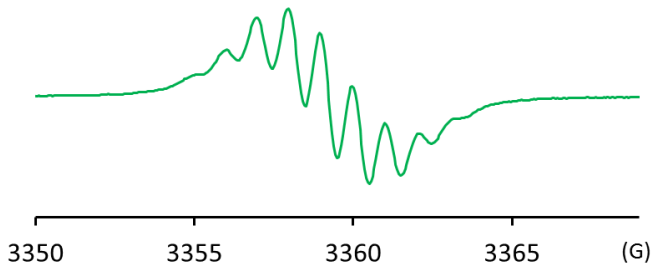

Figure S7. (a) Experimental EPR spectra of **[2a$^{\bullet+}$][Cl$^-$]** after heating for 7 days at 120°C under air (in solid state) at microwave frequency = 9.4328 GHz (measured with dichloromethane solution). (b) Experimental EPR spectra of **[2a$^{\bullet+}$][Cl$^-$]** after heating for 6 hours at 200°C under air (in solid state) at microwave frequency = 9.4337 GHz (measured with dichloromethane solution).

Cyclic Voltammetry

General information

Cyclic voltammograms were recorded at room temperature with a BioLogic SP-300 potentiostat. The working electrode was a glassy carbon disk (area = 0.02 cm^2), the reference electrode was Ag/AgCl (saturated), and the counter electrode was a platinum wire.

Cyclic voltammograms

(a)

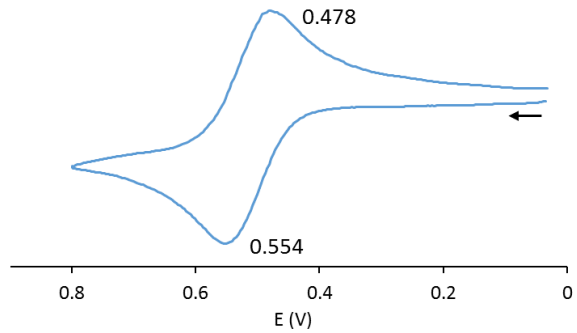

(b)

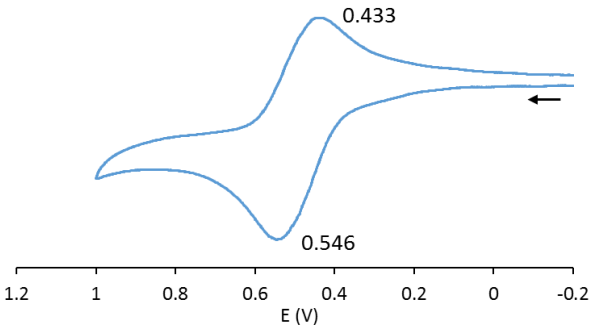

Figure S8. (a) Cyclic voltammogram of **[2a$^{\bullet+}$][BF_4^-]** (3.1 mM) in dry and degassed acetonitrile with Bu_4NPF_6 (0.1 M) as the supporting electrolyte (scan rate = 0.1 V/s). The cyclic voltammogram showed reversible one-electron redox potential at $E_{1/2}$ = 0.516 V versus Ag/AgCl (saturated) electrode, which corresponds to **2a**$^{\bullet+}$ + e^- ⇄ **2a**$^{2+}$. (b) Cyclic voltammogram of **[2b$^{\bullet+}$][BF_4^-]** (2.9 mM) in dry and degassed acetonitrile with Bu_4NPF_6 (0.1 M) as the supporting electrolyte (scan rate = 0.1 V/s). The cyclic voltammogram showed reversible one-electron redox potential at $E_{1/2}$ = 0.490 V versus Ag/AgCl (saturated) electrode, which corresponds to **2b**$^{\bullet+}$ + e^- ⇄ **2b**$^{2+}$.

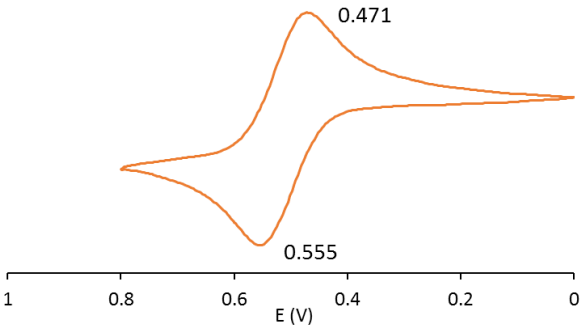

Figure S9. Cyclic voltammogram of $\mathbf{[2a^{2+}][BF_4^-]_2}$ (2.6 mM) in dry and degassed acetonitrile with Bu_4NPF_6 (0.1 M) as the supporting electrolyte (scan rate = 0.1 V/s). The cyclic voltammogram showed reversible one-electron redox potential at $E_{1/2}$ = 0.513 V versus Ag/AgCl (saturated) electrode, which corresponds to $\mathbf{2a^{\bullet+}} + e^- \rightleftarrows \mathbf{2a^{2+}}$.

UV-Vis Spectroscopy

General information

The UV-vis spectra were recorded at room temperature with Cary 6000i UV-Vis-NIR (Agilent Technologies) with quartz UV cell (path length = 10 mm).

Experimental and simulated UV-Vis spectra

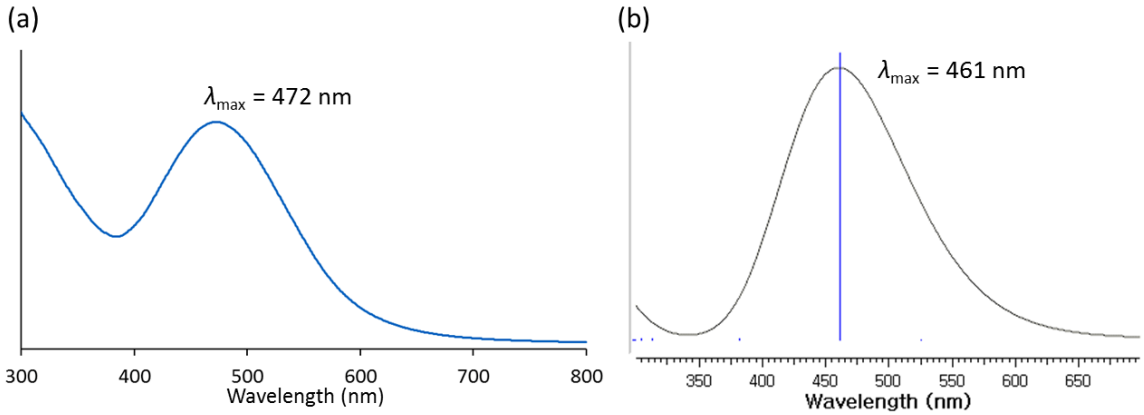

Figure S10. (a) UV-vis absorption of **[2a$^{\bullet+}$][Cl^{-}]** in distilled water. (b) Simulated UV-vis absorption from DFT calculation at M06/Def2-SV(P).

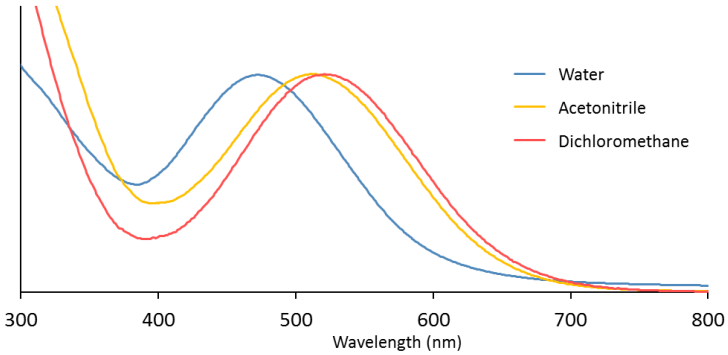

Figure S11. Comparison of UV-vis spectra of **[2a$^{\bullet+}$][Cl^{-}]** in distilled water (blue; λ_{max} = 472 nm), acetonitrile (yellow; λ_{max} = 510 nm), and dichloromethane (red; λ_{max} = 521 nm).

Stability

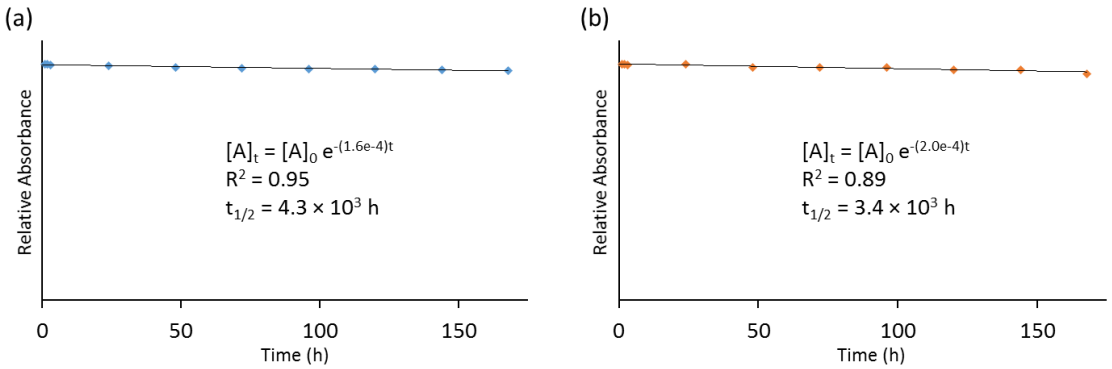

Figure S12. Decay of **[2a$^{\bullet+}$][Cl$^-$]** (0.16 mM; peak height at λ_{max} = 472 nm) in 0.1 M potassium phosphate buffer (pH 7.4) (a) without sodium ascorbate and (b) with excess sodium ascorbate (4 mM) monitored by UV-vis. Half-life was calculated by assuming 1st order kinetics.

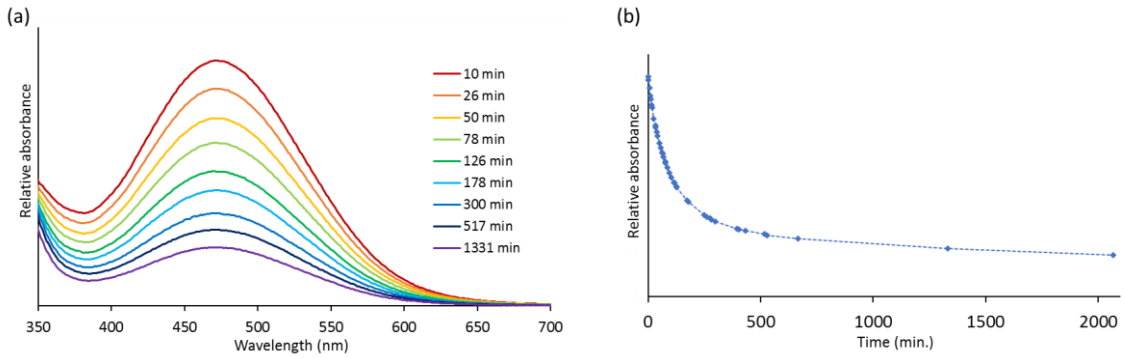

Figure S13. Decay of **[2a$^{\bullet+}$][Cl$^-$]** (0.16 mM; λ_{max} = 472 nm) in 0.1 M sulfuric acid. (a) Selected spectra. (b) Absorbance at 472 nm for 2000 minutes.

Mechanistic study

In a N_2 atmosphere glovebox, **[2a^{2+}][BF$_4^-$]$_2$** (2.5 mg) and IMesH$^+$Cl$^-$ (5.0 mg, ca. 5 eq.) were dissolved in dry acetonitrile (3 mL). The reaction mixture was monitored by UV-vis which showed the slow formation of **2a$^{\bullet+}$**.

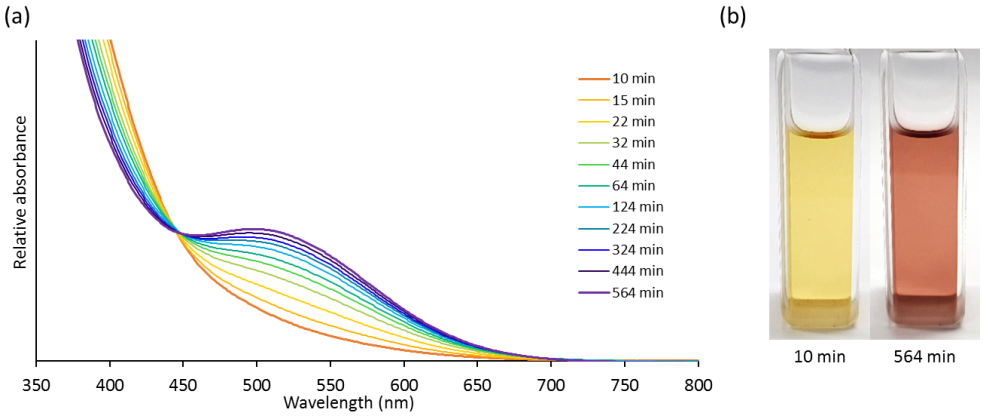

Figure S14. Monitoring of the formation of **2a$^{\bullet+}$** (corresponds to λ_{max} = 510 nm in acetonitrile) from the reaction between **[2a^{2+}][BF$_4^-$]$_2$** and IMesH$^+$Cl$^-$. (a) Selected spectra. (b) Color of the reaction mixture.

NMR

General information

^{1}H NMR spectra, proton decoupled ^{13}C NMR spectra (^{13}C{^{1}H}), and proton decoupled ^{19}F NMR spectra (^{19}F{^{1}H}) were recorded using a Bruker DRX 500 spectrometer operating at 500 MHz (for ^{1}H acquisitions), 126 MHz (for ^{13}C acquisitions), or 470 MHz (for ^{31}P acquisitions). Chemical shifts of ^{1}H and ^{13}C acquisitions were referenced to the residual solvent peaks (^{1}H: CD_3CN, δ = 1.94 ppm; ^{13}C: CD_3CN, δ = 118.26 ppm).[14]

NMR spectra

^{1}H, ^{13}C, ^{19}F NMR spectra of $[2a^{2+}][BF_4^-]_2$

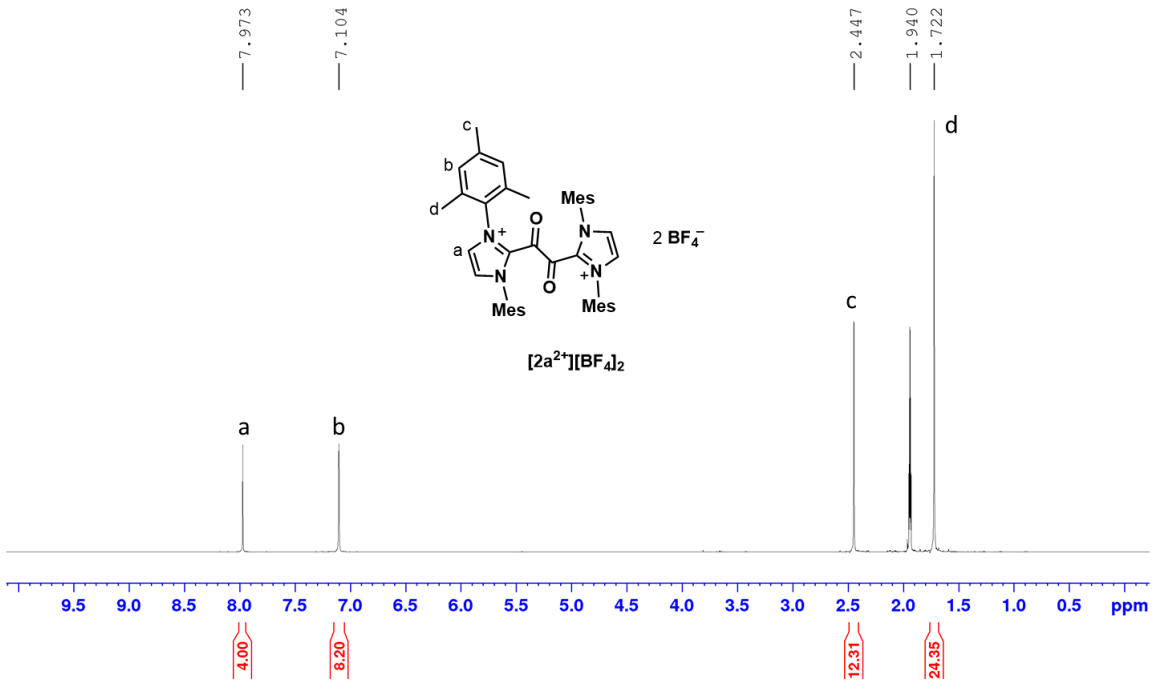

Figure S15. a) ^{1}H NMR spectrum and assignment of the signals for the compound $[2a^{2+}][BF_4^-]_2$.

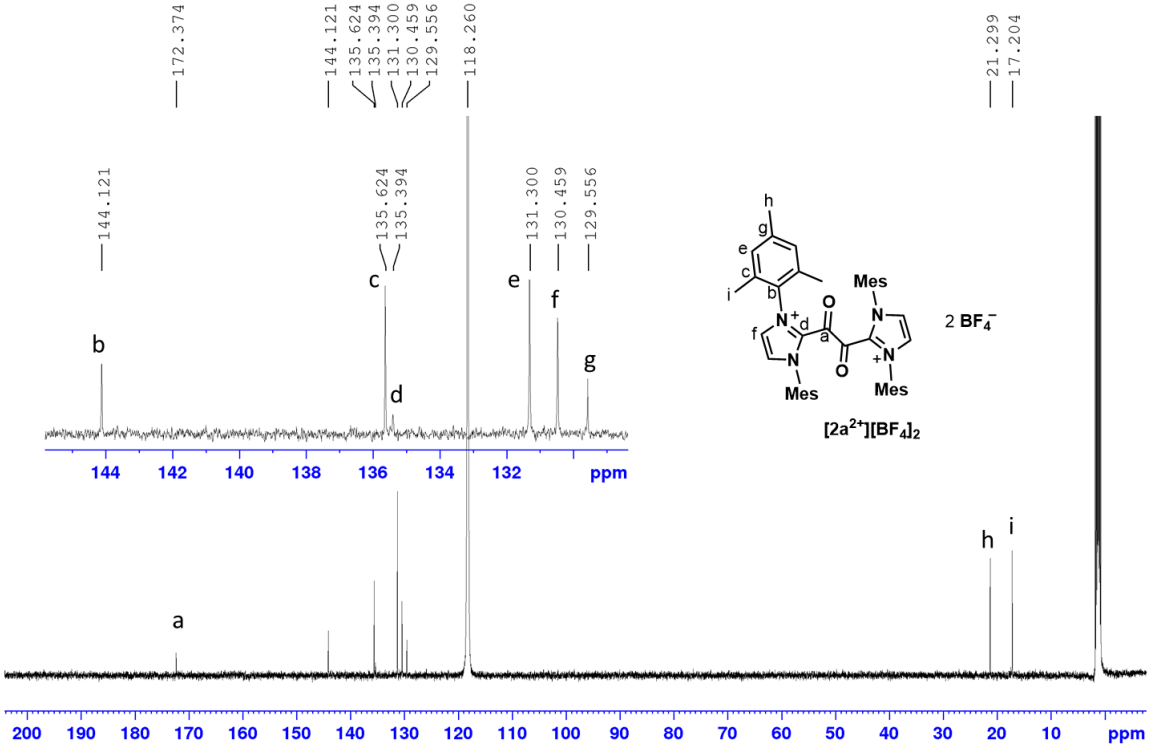

Figure S16. a) Proton decoupled ^{13}C NMR spectrum and assignment of the signals for the compound **[2a^{2+}][BF$_4^-$]$_2$**.

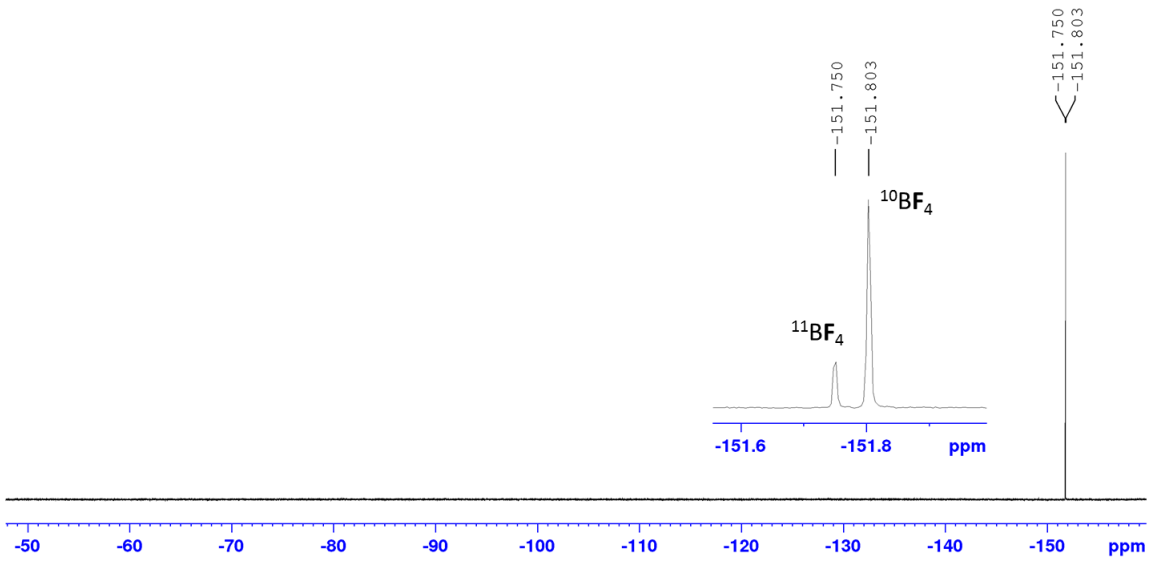

Figure S17. a) Proton decoupled ^{19}F NMR spectrum for the compound **[2a^{2+}][BF$_4^-$]$_2$**.

Relaxation experiments

Aqueous solution of the radical **[2a$^{\bullet+}$][Cl$^-$]** was added to a glass capillary and degassed. The capillary was sealed and placed in a NMR tube with benzene-d_6. T_1 and T_2 relaxation times were determined from inversion-recovery and Carr-Purcell-Meiboom-Gill experiment, respecti vely, using 300 MHz Bruker Avance III spectrometer with a magnetic field strength of 7 T under room temperature.

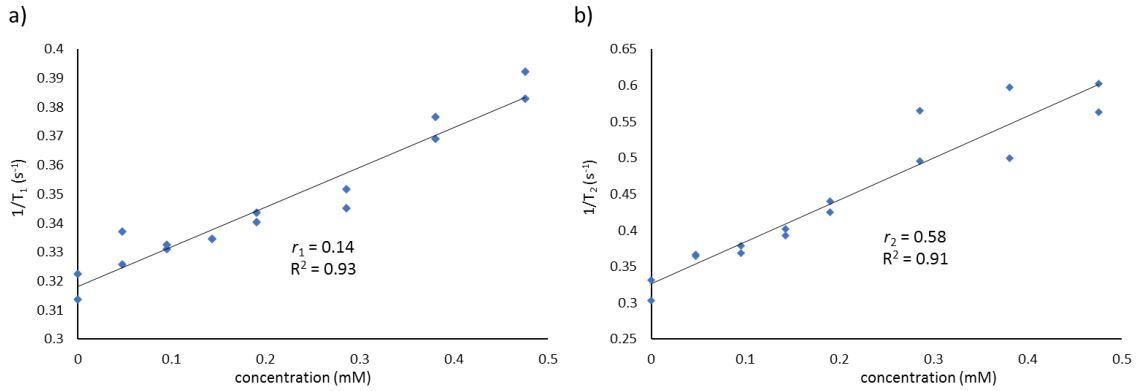

Figure S18. Calculation of a) T_1 relaxivity (r_1) and b) T_2 relaxivity (r_2) (in mM^{-1} S^{-1}).

Table S3. Data for T_1 and T_2 experiments.

T_1	Run 1	Run 2
0.00 mM	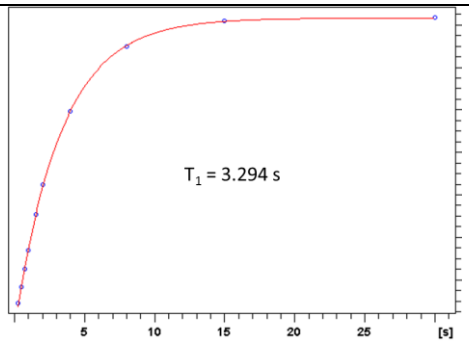	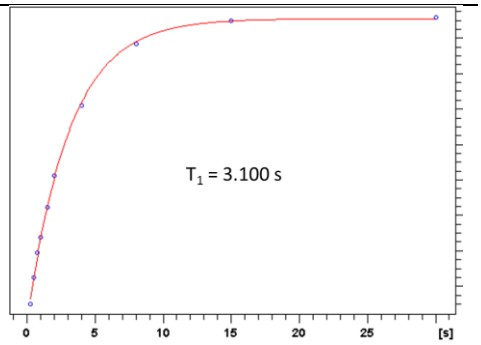
0.05 mM	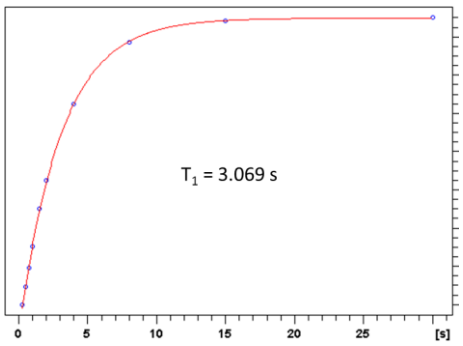	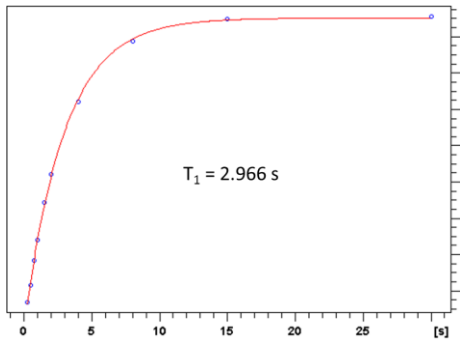

0.10 mM	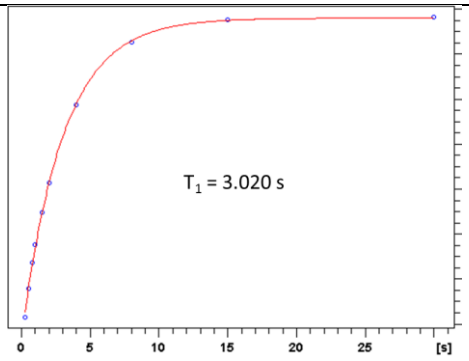	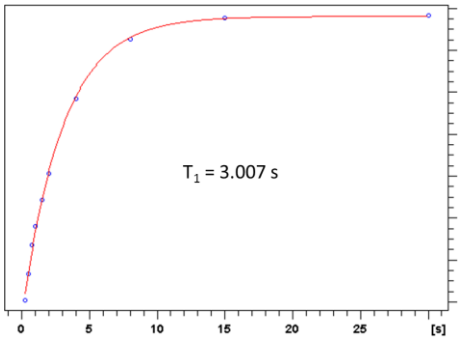
0.14 mM	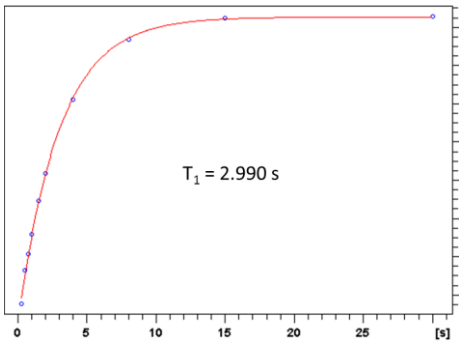	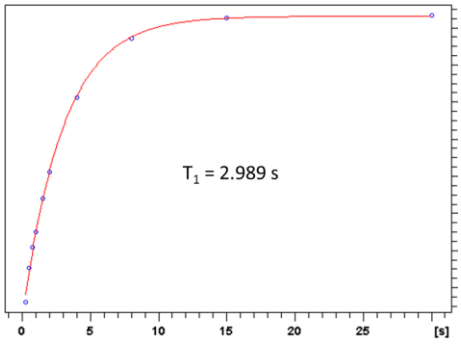
0.19 mM	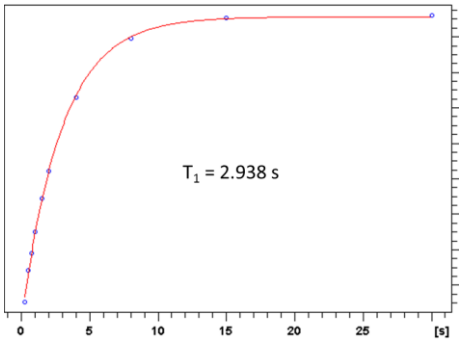	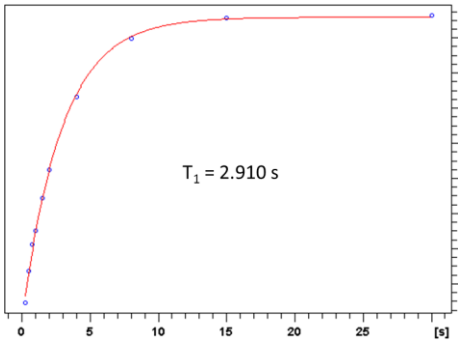
0.29 mM	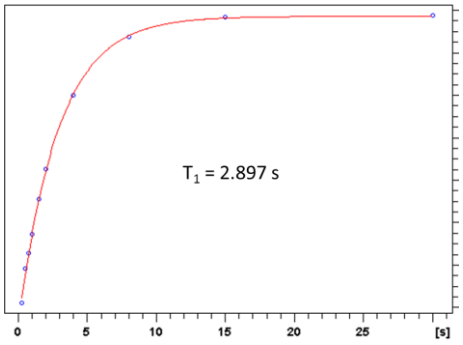	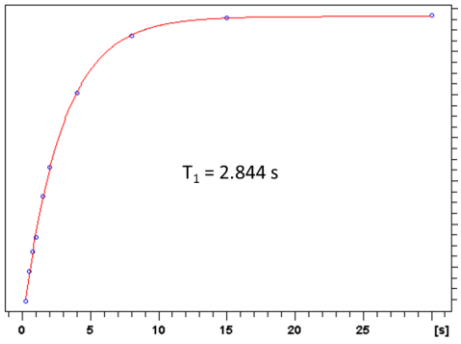
0.38 mM	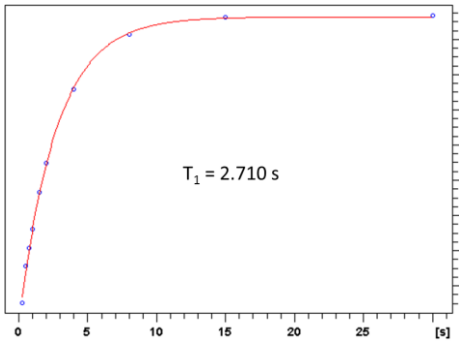	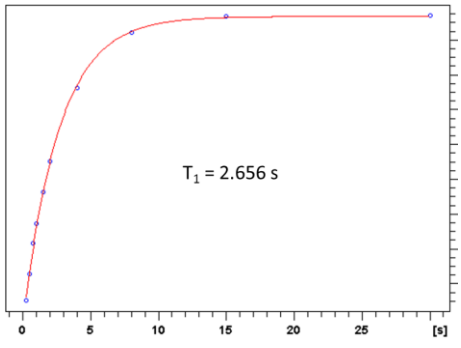

0.48 mM	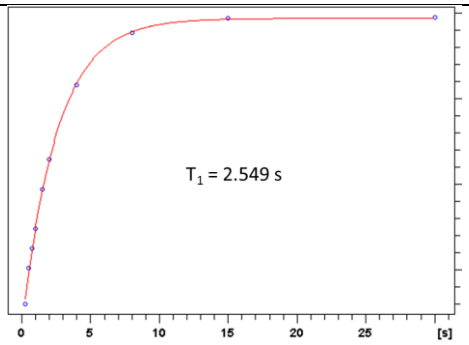	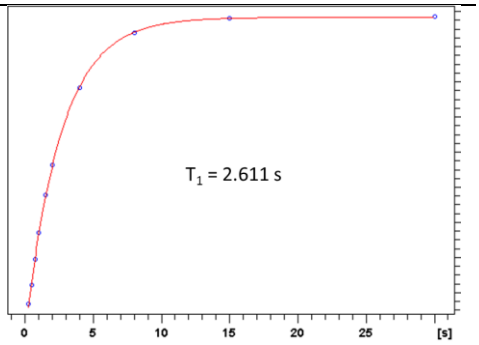
T_2	Run 1	Run 2
0.00 mM	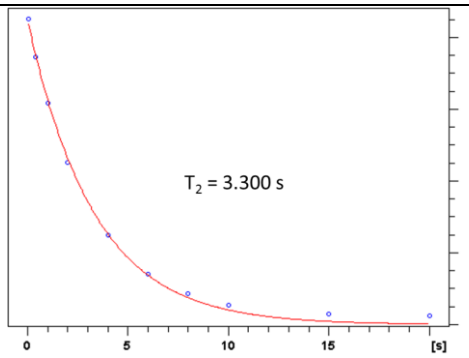	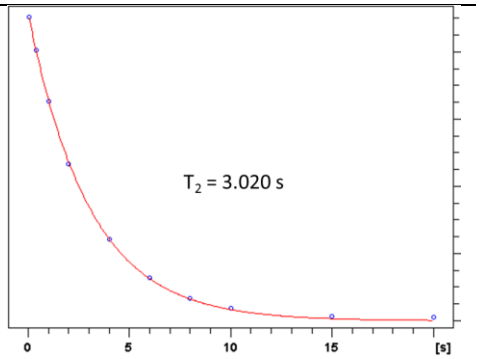
0.05 mM	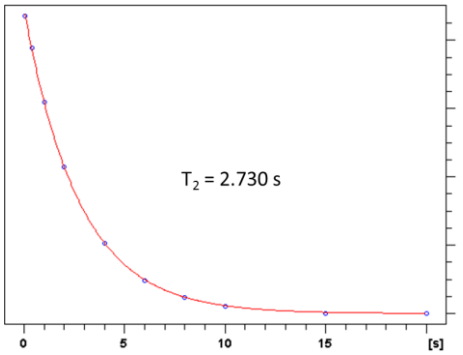	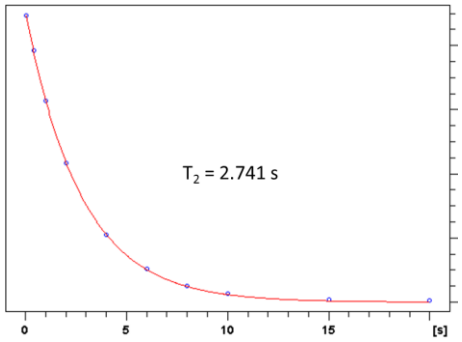
0.10 mM	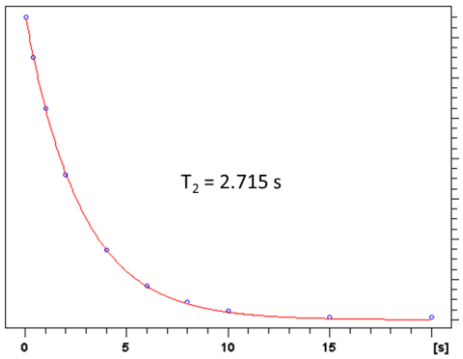	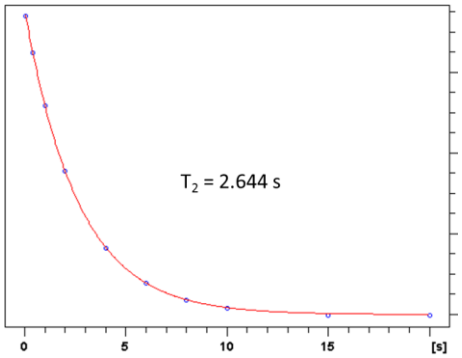
0.14 mM	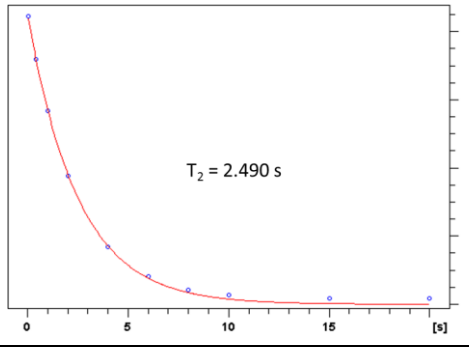	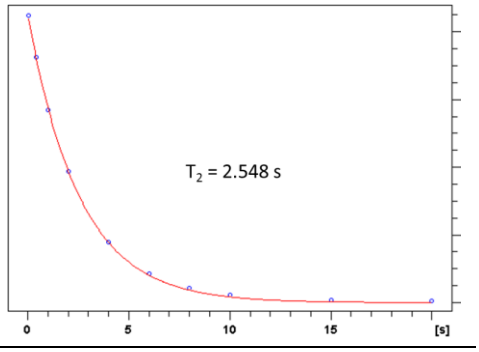

0.19 mM	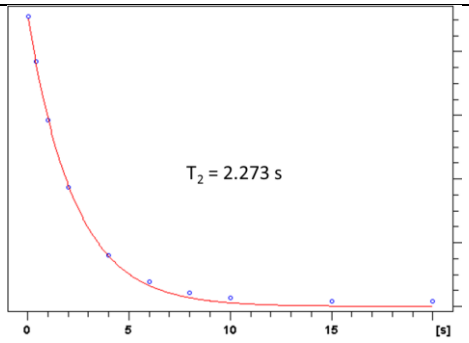	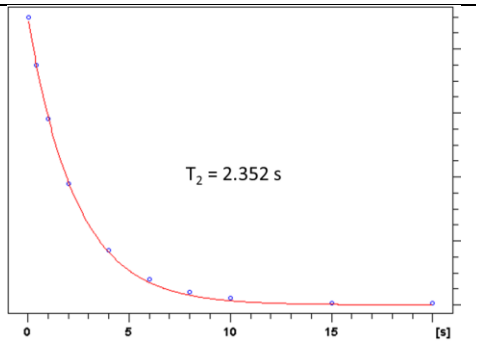
0.29 mM	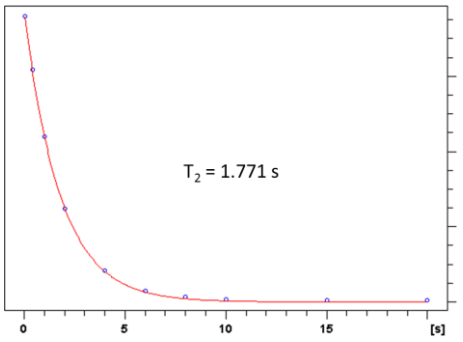	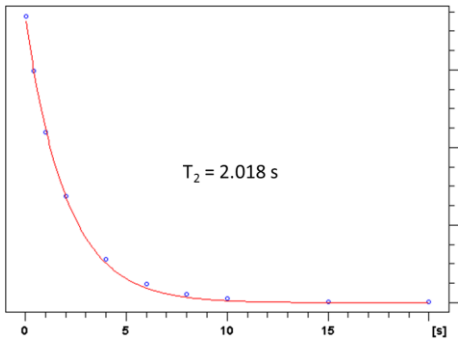
0.38 mM	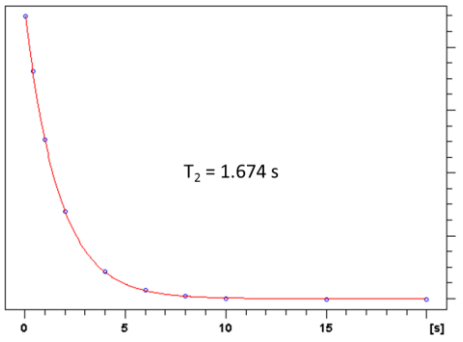	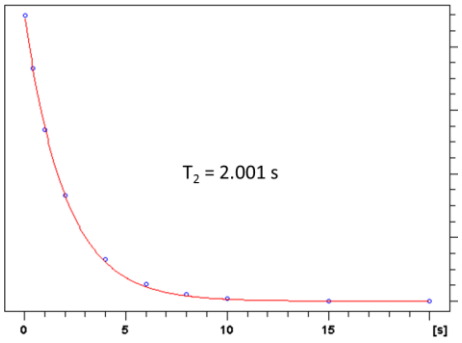
0.48 mM	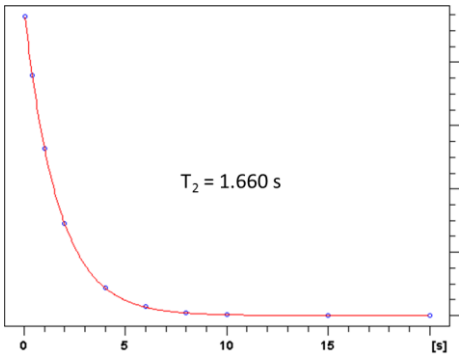	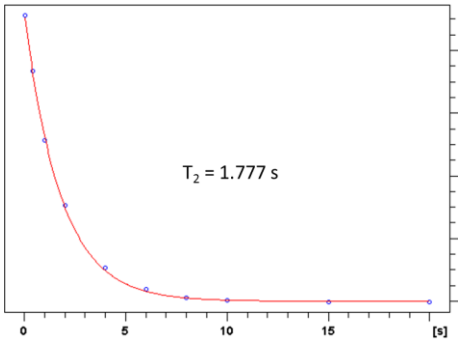

References

1. Bantreil, X., and Nolan, S.P. (2011). Synthesis of N-heterocyclic carbene ligands and derived ruthenium olefin metathesis catalysts. Nat. Protoc. *6*, 69-77.
2. Dong, Z., Pezzato, C., Sienkiewicz, A., Scopelliti, R., Fadaei-Tirani, F., and Severin, K. (2020). SET processes in Lewis acid–base reactions: the tritylation of N-heterocyclic carbenes. Chem. Sci. 10.1039/d0sc01278e.
3. Frisch, M.J., Trucks, G.W., Schlegel, H.B., Scuseria, G.E., Robb, M.A., Cheeseman, J.R., Scalmani, G., Barone, V., Petersson, G.A., Nakatsuji, H., Li, X., Caricato, M., Marenich, A.V., Bloino, J., Janesko, B.G., Gomperts, R., Mennucci, B., Hratchian, H.P., Ortiz, J.V., Izmaylov, A.F., Sonnenberg, J.L., Williams-Young, D., Ding, F., Lipparini, F., Egidi, F., Goings, J., Peng, B., Petrone, A., Henderson, T., Ranasinghe, D., Zakrzewski, V.G., Gao, J., Rega, N., Zheng, G., Liang, W., Hada, M., Ehara, M., Toyota, K., Fukuda, R., Hasegawa, J., Ishida, M., Nakajima, T., Honda, Y., Kitao, O., Nakai, H., Vreven, T., Throssell, K., Jr., J.A.M., Peralta, J.E., Ogliaro, F., Bearpark, M.J., Heyd, J.J., Brothers, E.N., Kudin, K.N., Staroverov, V.N., Keith, T.A., Kobayashi, R., Normand, J., Raghavachari, K., Rendell, A.P., Burant, J.C., Iyengar, S.S., Tomasi, J., Cossi, M., Millam, J.M., Klene, M., Adamo, C., Cammi, R., Ochterski, J.W., Martin, R.L., Morokuma, K., Farkas, O., Foresman, J.B., and Fox, D.J. (2016). Gaussian 16, Revision A.03 (Gaussian, Inc., Wallingford CT).
4. Zhao, Y., and Truhlar, D.G. (2007). The M06 suite of density functionals for main group thermochemistry, thermochemical kinetics, noncovalent interactions, excited states, and transition elements: two new functionals and systematic testing of four M06-class functionals and 12 other functionals. Theor. Chem. Acc. *120*, 215-241.
5. Weigend, F., and Ahlrichs, R. (2005). Balanced basis sets of split valence, triple zeta valence and quadruple zeta valence quality for H to Rn: Design and assessment of accuracy. Phys. Chem. Chem. Phys. *7*, 3297-3305.
6. Lu, T., and Chen, F. (2012). Multiwfn: a multifunctional wavefunction analyzer. J. Comput. Chem. *33*, 580-592.
7. Knizia, G. (2013). Intrinsic Atomic Orbitals: An Unbiased Bridge between Quantum Theory and Chemical Concepts. J. Chem. Theory Comput. *9*, 4834-4843.
8. Knizia, G., and Klein, J.E. (2015). Electron flow in reaction mechanisms--revealed from first principles. Angew. Chem. Int. Ed. *54*, 5518-5522.
9. Dolomanov, O.V., Bourhis, L.J., Gildea, R.J., Howard, J.A.K., and Puschmann, H. (2009). OLEX2: a complete structure solution, refinement and analysis program. J. Appl. Crystallogr. *42*, 339-341.
10. Sheldrick, G.M. (2015). SHELXT - integrated space-group and crystal-structure determination. Acta. Cryst. *A71*, 3-8.
11. Sheldrick, G.M. (2015). Crystal structure refinement with SHELXL. Acta. Cryst. *C71*, 3-8.
12. Rees, B., Jenner, L., and Yusupov, M. (2005). Bulk-solvent correction in large macromolecular structures. Acta. Cryst. *D61*, 1299-1301.
13. Stoll, S., and Schweiger, A. (2006). EasySpin, a comprehensive software package for spectral simulation and analysis in EPR. J. Magn. Reson. *178*, 42-55.
14. Fulmer, G.R., Miller, A.J.M., Sherden, N.H., Gottlieb, H.E., Nudelman, A., Stoltz, B.M., Bercaw, J.E., and Goldberg, K.I. (2010). NMR Chemical Shifts of Trace Impurities: Common Laboratory Solvents, Organics, and Gases in Deuterated Solvents Relevant to the Organometallic Chemist. Organometallics *29*, 2176-2179.